3-2013

Pseudomonas HopU1 modulates plant immune receptor levels by blocking the interaction of their mRNAs with GRP7

Valerie Nicaise
The Sainsbury Laboratory, Norwich Research Park, Norwich, UK

Anna Joe
University of Nebraska-Lincoln

Byeong-Ryool Jeong
University of Nebraska - Lincoln, bjeong2@unl.edu

Christin Korneli
University of Bielefeld, Germany

Freddy Boutrot
The Sainsbury Laboratory, Norwich Research Park, Norwich, UK

See next page for additional authors

The EMBO Journal
EMBO J. 32(5): 701-712

Pseudomonas HopU1 modulates plant immune receptor levels by blocking the interaction of their mRNAs with GRP7

Valerie Nicaise[1]*, Anna Joe[2]*, Byeong-ryool Jeong[3]†, Christin Korneli[4], Freddy Boutrot[1], Isa Westedt[1]‡, Dorothee Staiger[4], James R Alfano[a3], Cyril Zipfel[b1]

1. The Sainsbury Laboratory, Norwich Research Park, Norwich, UK

2. School of Biological Sciences, Center for Plant Science Innovation, University of Nebraska, Lincoln, NE, USA

3. Department of Plant Pathology, Center for Plant Science Innovation, University of Nebraska, Lincoln, NE, USA

4. Molecular Cell Physiology and Cebitec, University of Bielefeld, Bielefeld, Germany

a. Department of Plant Pathology, Center for Plant Science Innovation, University of Nebraska, Lincoln, NE 68588-0660, USA. Tel.:+1 402 472 0395; Fax:+1 402 472 3139; E-mail: jalfano2@unl.edu

b. The Sainsbury Laboratory, Norwich Research Park, Colney Lane, Norwich NR4 7UH, UK. Tel.:+44 1603 452056; Fax:+44 1603 450011; E-mail: cyril.zipfel@tsl.ac.uk

*. These authors contributed equally to this work.

†. Present address: Biology Department, Creighton University, 2500 California Plaza, Omaha, NE 68178, USA.

‡. Present address: Research Center for Infectious Diseases, University of Wuerzburg, 97080 Wuerzburg, Germany.

DOI: 10.1038/emboj.2013.15
Published in print: 06 March 2013
Published online: 08 February 2013

Abstract

Pathogens target important components of host immunity to cause disease. The *Pseudomonas syringae* type III-secreted effector HopU1 is a mono-ADP-ribosyltransferase required for full virulence on *Arabidopsis thaliana*. HopU1 targets several RNA-binding proteins including GRP7, whose role in immunity is still unclear. Here, we show that GRP7 associates with translational components, as well as with the pattern recognition receptors FLS2 and EFR. Moreover, GRP7 binds specifically *FLS2* and *EFR* transcripts *in vivo* through its RNA recognition motif. HopU1 does not affect the protein–protein associations between GRP7, FLS2 and translational components. Instead, HopU1 blocks the interaction between GRP7 and *FLS2* and *EFR* transcripts *in vivo*. This inhibition correlates with reduced FLS2 protein levels upon *Pseudomonas* infection in a HopU1-dependent manner. Our results reveal a novel virulence strategy used by a microbial effector to interfere with host immunity.

Pseudomonas HopU1 modulates plant immune receptor levels by blocking the interaction of their mRNAs with GRP7

The *Pseudomonas* virulence factor HopU1 mono-ADP-ribosylates the plant RNA-binding protein GRP7 protein to inhibit its binding to immune receptor mRNAs, leading to the suppression of receptor protein synthesis and hence host immunity.

Introduction

An important aspect of innate immunity is the perception of pathogen-associated molecular patterns (PAMPs) by specific pattern recognition

receptors (PRRs) leading to PAMP-triggered immunity (PTI; Dodds and Rathjen, 2010; Segonzac and Zipfel, 2011). In Arabidopsis thaliana, the leucine-rich repeat receptor kinases (LRR-RKs) FLS2 and EFR recognize bacterial flagellin (or its derived peptide flg22) and EF-Tu (or its derived peptide elf18), respectively (Gomez-Gomez and Boller, 2000; Zipfel et al, 2006), while perception of fungal chitin depends on the LysM-RK CERK1 (Miya et al, 2007; Wan et al, 2008). In addition to its role in chitin perception, CERK1 is required for peptidoglycan perception (Willmann et al, 2011). Perception of flg22, elf18 or chitin induces a series of early immune responses, including a rapid burst of reactive oxygen species (ROS), phosphorylation events, gene expression, as well as late responses such as callose deposition at the plant cell wall and resistance to pathogens (Segonzac and Zipfel, 2011). Plant PRRs are key to immunity, as their inhibition or loss of function leads to enhanced susceptibility to adapted and non-adapted pathogens (Segonzac and Zipfel, 2011; Willmann et al, 2011).

Pathogens must block or avoid PTI to cause disease. A potent strategy to inhibit PTI is via the action of secreted effectors delivered into the host cells leading to effector-triggered susceptibility (ETS; Dodds and Rathjen, 2010). The genome of the phytopathogenic bacterium Pseudomonas syringae pv. tomato DC3000 (Pto DC3000) encodes >30 type III-secreted effectors (T3SEs). Recently, several T3SEs from different P. syringae strains were shown to be virulence factors. Corresponding host targets have been identified only for a few of them, but they revealed that T3SEs interfere with key components of PTI (Block and Alfano, 2011). For instance, AvrPto is a kinase inhibitor that blocks PTI signalling by interfering with the activation of PRRs and/or the complex formation of PRRs with their associated proteins (Xing et al, 2007; Shan et al, 2008; Xiang et al, 2008, 2011). AvrPtoB is a multifunctional protein carrying E3 ubiquitin ligase

activity that leads to the degradation of several PRRs and the inhibition of the PRR-associated LRR-RK BAK1 (Gohre et al, 2008; Shan et al, 2008; Gimenez-Ibanez et al, 2009; Cheng et al, 2011; Zeng et al, 2012). Other Pto DC3000 T3SEs target signalling components downstream of PRR activation (Block and Alfano, 2011; Feng et al, 2012).

The Pto DC3000 T3SE HopU1 is a mono-ADP-ribosyltransferase (mono-ADP-RT) required for full virulence in Arabidopsis (Fu et al, 2007). Ectopic expression of HopU1 in A. thaliana suppresses callose deposition induced by flg22 in a manner dependent on its mono-ADP-RT activity (Fu et al, 2007). HopU1 targets at least five different A. thaliana RNA-binding proteins (RBPs), including Glycine-Rich Protein 7 (GRP7) and GRP8 (Fu et al, 2007). HopU1 mono-ADP-ribosylates an arginine at position 49 (R49) located in the conserved ribonucleoprotein consensus sequence 1 (RNP-1) motif of the RNA recognition motif (RRM) of GRP7, and this modification affects GRP7's ability to bind RNA in vitro (Jeong et al, 2011). Although HopU1 targets several RBPs, grp7 null mutant plants produce less ROS and callose in response to flg22, elf18 and chitin (Fu et al, 2007; Jeong et al, 2011), indicating that GRP7 regulates both early and late PAMP responses. In addition, grp7 plants are more susceptible to Pto DC3000 (Fu et al, 2007; Jeong et al, 2011). A mutation in R49 blocks the ability of GRP7 to complement these phenotypes (Jeong et al, 2011). These results demonstrate the importance of GRP7 in plant innate immunity and the potency of mono-ADP-ribosylation to block GRP7 function. However, as in the case for many targets of pathogenic effectors, the exact role of GRP7 in innate immunity and therefore the molecular mechanism underlying PTI suppression by HopU1 are still unclear.

Here, we illustrate a function for GRP7 in PTI that is inhibited by HopU1.

We show that GRP7 associates with translational components in vivo, and more surprisingly that GRP7 associates with the PRRs FLS2 and EFR. However, HopU1 does not affect the associations between GRP7, FLS2 and translational components. Instead, we reveal that GRP7 binds FLS2 and EFR mRNA in vivo, and that HopU1 blocks this interaction. The FLS2 and EFR transcripts provide the first examples of in vivo targets for GRP7 with a clear biological function. This inhibition correlates with reduced FLS2 protein levels in planta upon infection with Pto DC3000 in a HopU1-dependent manner. Our results reveal a novel virulence strategy used by a microbial effector to interfere with host immunity.

Results

Modulation of GRP7 level and activity affects early and late immune responses

Previous results conclusively showed that loss of GRP7 impairs PTI and resistance to Pto DC3000 infection (Fu et al, 2007; Jeong et al, 2011). To investigate the consequences of ectopic GRP7 expression, we monitored PTI and pathogen response in transgenic A. thaliana plants expressing untagged GRP7 under the control of the constitutive promoter 35S (GRP7ox lines) (Streitner et al, 2008). An immunoblot analysis using a specific anti-GRP7 antibody confirmed higher GRP7 levels in transgenic homozygous GRP7ox plants in comparison to the wild-type (WT) Col-2 ecotype (Supplementary Figure S1). A. thaliana Col-2 (WT) and GRP7ox plants were treated with flg22, elf18 or chitin, which resulted in substantially higher ROS production in GRP7ox plants compared to WT (Figure 1A). Similarly, callose deposition was increased in GRP7ox plants compared to WT plants after all three treatments (Figure 1B).

The A. thaliana GRP7ox plants were used in pathogenicity assays with Pto DC3000 or the Pto DC3000 hrcC$^-$ mutant that does not secrete any T3SEs and is therefore severely hypo-virulent. Plants were spray inoculated and bacteria were enumerated at 0 and 4 days after inoculation. Interestingly, GRP7ox plants were more resistant to infection by Pto DC3000 than WT plants (Figures 1C and D). The Pto DC3000 hrcC$^-$ mutant exhibited unaltered growth on GRP7ox plants. This may be due to the strongly reduced virulence of the Pto DC3000 hrcC$^-$ mutant to which the endogenous GRP7 seems to be sufficient to confer high resistance. The increased resistance to Pto DC3000 infection observed in plants overexpressing GRP7 clearly demonstrates its important role in innate immunity.

GRP7 is required for full immunity to Pto DC3000 WT and hrcC$^-$, and HopU1 targets GRP7 (Fu et al, 2007; Jeong et al, 2011). To assess the extent to which HopU1 inhibits PTI responses, we analysed early and late responses triggered by flg22 in transgenic A. thaliana lines constitutively expressing HopU1 C-terminally tagged with haemagglutinin (HA) under the control of the 35S promoter (Fu et al, 2007). In HopU1 plants, the ROS burst induced by flg22 and elf18 treatment was reduced compared to WT plants (Supplementary Figure S2A). Next, we confirmed that HopU1 leaves exhibit less callose deposition upon flg22 treatment (Supplementary Figure S2B; Fu et al, 2007). The reduced flg22 responsiveness of the HopU1 plants correlated with reduced FLS2 protein levels observed in three out of four independent biological experiments (Supplementary Figure S2C). These results were further validated using A. thaliana transgenic lines expressing HopU1-HA under the control of an estradiol-inducible promoter (ind_HopU1) (Supplementary Figures S2D and E). Together, this

demonstrates that HopU1 affects both early and late flg22-induced responses.

To test whether in planta HopU1 expression affects A. thaliana disease resistance, we assayed bacterial growth after spray inoculation with the Pto DC3000 strains WT, hrcC^{-} or ΔhopU1 that is hypo-virulent (Fu et al, 2007). HopU1 plants were more susceptible to all the strains tested (Supplementary Figure S2F), albeit to a lesser extent than fls2 null mutant plants consistent with the reduced flg22 sensitivity of HopU1 plants (Supplementary Figures S2A–E). Consistent with the notion that GRP7 is a main target of HopU1 in reducing plant immunity, GRP7ox plants were as resistant to Pto DC3000 as WT plants to Pto DC3000 ΔhopU1 (Supplementary Figure S2G). These results, together with previous results (Fu et al, 2007; Jeong et al, 2011), indicate that the abundance and/or activity of GRP7 are both required and limited for triggering optimal early and late PTI responses.

GRP7 associates with the immune receptors FLS2 and EFR at the plasma membrane

The importance of GRP7 for early PTI responses suggests that GRP7 may affect directly PRRs and/or associated proteins, or indirectly the expression and/or biogenesis of such proteins.

Notably, we identified GRP7 in an unbiased yeast two-hybrid screen for EFR-interacting proteins (Supplementary Figure S3A). Importantly, we could confirm this interaction in co-immunoprecipitation experiments after transient co-expression of EFR and GRP7 as C-terminally tagged fusion proteins with HA and enhanced green fluorescent protein (GFP) tags (EFR-3 × HA and GRP7-eGFP, respectively) in Nicotiana benthamiana (Figure 2A). Similarly, GRP7 and FLS2 also interacted when transiently co-expressed as

fusion proteins (FLS2-3 × myc and GRP7-eGFP) in N. benthamiana (Figure 2B). However, GRP7-eGFP did not interact under similar conditions with the LRR-RK BAK1 (BAK1-HA) (Figure 2C), which is an important positive regulator of PTI responses downstream of FLS2 and EFR (Chinchilla et al, 2007; Heese et al, 2007; Roux et al, 2011).

We confirmed the GRP7–FLS2 association by co-immunoprecipitation in an A. thaliana transgenic line expressing GRP7 C-terminally tagged with a GFP epitope (GRP7-GFP) under the control of the 35S promoter (Kim et al, 2008) and using an anti-FLS2 antibody recognizing the native FLS2 protein (Figure 2D). The GRP7–FLS2 interaction occurred independently of elicitation and was unaltered by flg22 treatment (Figure 2D). The presence of EFR and FLS2 proteins that may correspond to their glycosylated forms (migrating at ~150 kDa and ~175 kDa, respectively Nekrasov et al, 2009; Haweker et al, 2010) in the GRP7 immunoprecipitates (Figures 2A, B and D) suggests that the association between GRP7 and PRRs occurs at the plasma membrane once the mature and functional PRRs have migrated through the secretory pathway.

GRP7-GFP shows a nucleo-cytoplasmic subcellular localization in A. thaliana, tobacco (Nicotiana tabacum) and N. benthamiana cells upon stable or transient expression (Supplementary Figures S4A and B; Ziemienowicz et al, 2003; Fu et al, 2007; Kim et al, 2008; Lummer et al, 2011). Bimolecular fluorescence complementation (BiFC) experiments using split-yellow fluorescent protein (YFP) following transient expression in N. benthamiana suggest that GRP7 and FLS2 closely associate (Figure 2E). This interaction occurs most likely at the plasma membrane, as indicated by the presence of the reconstituted YFP signal in typical cell wall–plasma membrane connections (called Hechtian strands) after cell plasmolysis

(arrows in Figure 2E). An interaction at the cell periphery between GRP7 and EFR could also be observed (Supplementary Figure S3B).

GRP7 associates with translational components

In exploratory experiments to identify GRP7 interactors in planta by immunoprecipitation using an A. thaliana transgenic line expressing GRP7 C-terminally tagged with HA under the control of its native promoter (GRP7-HA) (Jeong et al, 2011), we identified by mass-spectrometry analysis of the GRP7-HA immunoprecipitates several components of the 43S complex involved in protein translation (Supplementary Table S1). Before the initiation of active translation, the 43S complex recruits both mRNAs and ribosomes, and is composed of several initiation factors in addition to the cap-binding protein eIF4E and the ribosomal 40S subunit (Pestova et al, 2001).

Co-immunoprecipitation experiments using the A. thaliana GRP7-GFP transgenic line (Kim et al, 2008) and specific antibodies further revealed the presence of eIF4E and the ribosomal subunit S14 in complex with GRP7 (Figure 3). We used here the GRP7-GFP line for consistency with previous targeted co-immunoprecipitation experiments (Figure 2). Interestingly, slower migrating bands of eIF4E were enriched in GRP7-GFP immunoprecipitates in comparison to the main form detected in the input (see asterisks in Figure 3). Strikingly, treatment with flg22 induced the dissociation of elF4E and S14 from the GRP7 complex (Figure 3), indicating a potential dynamic link between GRP7, ligand-activated PRRs and components of the translational machinery.

HopU1 does not affect interactions between GRP7, PRRs and translational components

Next, we tested if HopU1 could directly affect FLS2 or the GRP7–FLS2 interaction. HopU1 did not interact with FLS2 in vivo as determined by co-immunoprecipitation and split-YFP experiments in N. benthamiana (Supplementary Figures S5A and B). Consistently, HopU1 did not mono-ADP-ribosylate FLS2 in vitro (Supplementary Figure S5C).

Although HopU1 directly interacts with GRP7 in vivo (Supplementary Figure S6), HopU1 did not affect the interaction between GRP7 and FLS2 in an A. thaliana transgenic line expressing both GRP7-GFP and HopU1-HA (Figure 4). In addition, HopU1 did not interfere, at least qualitatively, with the association or ligand-induced dissociation between GRP7-GFP and either elF4E or S14 (Supplementary Figure S7). Therefore, the effect of HopU1 on PTI responses is most likely not mediated by direct inhibition of PRRs or protein–protein interactions with GRP7.

GRP7 associates with FLS2 and EFR transcripts in planta

Next, we investigated the role of GRP7 in PTI in relation to its capacity to bind RNA by testing if GRP7 could bind PRR transcripts. Quantitative RNA-immunoprecipitation assays using the A. thaliana GRP7-HA (Jeong et al, 2011) transgenic line revealed that GRP7 binds FLS2 mRNAs in vivo independently of flg22 treatment (Figure 5A). As positive controls, we confirmed that GRP7 binds its own transcripts as well as transcripts of its closest paralogue GRP8 (Figure 5A), as previously reported in vitro (Staiger et al, 2003; Schoning et al, 2008). GRP7 binds the 3′-UTR of its own transcript and of the GRP8 mRNA (Schoning et al, 2007). Similarly, we identified the 3′-UTR as a binding region of GRP7 in the FLS2 mRNA (Figures 5B and C). In addition to the FLS2 mRNA, GRP7 could also bind the EFR transcript in vivo (Supplementary Figure S8A), consistent with the importance of GRP7 for responses triggered by both flg22 and elf18 (Jeong

et al, 2011; Figure 1). However, transcripts of the regulatory LRR-RK BAK1 were not enriched in GRP7 immunoprecipitates (Figure 5A; Supplementary Figure S8A), revealing a certain degree of specificity. Interestingly, GRP8, which is also targeted by HopU1 (Fu et al, 2007), is also able to bind FLS2 and EFR mRNAs (Supplementary Figure S9). These results demonstrate that GRP7, as well as GRP8, bind transcripts of the important PRRs FLS2 and EFR.

HopU1 disrupts the association between GRP7 and PRR transcripts

Next, we investigated if HopU1 could affect the ability of GRP7 to bind its target mRNAs, including FLS2 and EFR transcripts. Using an A. thaliana transgenic line expressing both GRP7-GFP and HopU1-HA in quantitative RNA-immunoprecipitation assays, we found that the amount of FLS2 and EFR transcripts bound to GRP7-GFP was strongly reduced in the presence of HopU1 (Figure 6A; Supplementary Figure S8A). A similar effect was observed on the interaction between GRP7 and its own mRNA (Figure 6A; Supplementary Figure S8A). Furthermore, a GRP7(R49K) variant, which carries a mutation in a conserved arginine residue within the RRM RNA-binding domain that is mono-ADP-ribosylated by HopU1 (Jeong et al, 2011), is strongly impaired in its ability to bind FLS2, EFR, GRP7 and GRP8 transcripts (Figure 6B; Supplementary Figure S8B). Furthermore, ADP ribosylation of GRP7 by HopU1 (but not by the catalytically inactive HopU1DD variant; Fu et al, 2007; Jeong et al, 2011) completely blocks the binding of GRP7 to the 3′-UTR of FLS2 mRNA in vitro (Figure 6C). Together, our results suggest that the mono-ADP ribosylation of GRP7 by HopU1 disrupts in planta the ability of GRP7 to bind mRNAs of the PRRs FLS2 and EFR.

HopU1 inhibits the pathogen-induced FLS2 protein accumulation

during Pseudomonas infection

Because HopU1 inhibits GRP7–FLS2 mRNA binding (Figure 6), we asked whether HopU1's action could ultimately affect FLS2 protein levels after translocation into A. thaliana cells during Pto DC3000 infection, which would correspond to the most biologically relevant observation. We observed that the amount of FLS2 protein increases (3.5- to 3.8-fold) over 24 h in leaves infected with Pto DC3000 hrcC$^-$ (unable to secrete any T3SEs and therefore unable to dampen PTI) (Figure 7A), consistent with the previous observation that the expression of FLS2, EFR and other potential PRR-encoding genes is PAMP inducible (Zipfel et al, 2004, 2006). Notably, this PAMP-induced accumulation is attenuated by T3SEs (Figure 7A; compare hrcC$^-$ with WT). However, this T3SE-mediated suppression was much less marked after inoculation with Pto DC3000 ΔhopU1 (Figure 7A; compare ΔhopU1 with WT). Importantly, expression of HopU1 in trans on a plasmid in Pto DC3000 ΔhopU1 restored the inhibition of FLS2 accumulation during infection, while trans-complementation with the catalytically inactive HopU1DD variant (Fu et al, 2007; Jeong et al, 2011) did not (Figure 7B). In addition, HopU1 does not affect BAK1 levels during infection (Supplementary Figure S10); consistent with our previous finding that GRP7 does not bind BAK1 mRNA (Figures 5 and 6; Supplementary Figure S8).

Notably, while the amount of cellular FLS2 mRNA increased during the first hours of infection with Pto DC3000 hrcC$^-$, it decreased to a similar level upon infection with Pto DC3000 WT and ΔhopU1 (Figure 7C). The contrasting regulation and sensitivity to HopU1 of FLS2 mRNA and protein levels during infection further demonstrate that HopU1 regulates FLS2 post-transcriptionally, while other T3SEs already regulate FLS2 at the

transcriptional level. Consistent with FLS2 being an important virulence target for HopU1, we found that deletion of the flagellin-encoding gene fliC in the ΔhopU1 background (Pto DC3000 ΔhopU1 ΔfliC) suppresses the virulence defect of Pto DC3000 ΔhopU1 and restores the virulence of Pto DC3000 ΔhopU1 ΔfliC to a comparable level as Pto DC3000 ΔfliC on WT A. thaliana plants (Figure 7D). Together, these results indicate that HopU1 strongly affects the increased accumulation of FLS2 protein level normally observed during the first hours of A. thaliana infection by Pto DC3000.

Discussion

Several animal and plant pathogenic bacteria use toxins or T3SEs that possess mono-ADP-RT activity as major virulence factors via the targeting of distinct host proteins (Deng and Barbieri, 2008; Block and Alfano, 2011). The mono-ADP-RT toxins diphtheria toxin (DT) from Corynebacterium diphtheriae, ExoA from P. aeruginosa and cholix toxin (CT) from Vibrio cholerae interact with the eukaryotic elongation factor eEF2 as a unique specific host target (Deng and Barbieri, 2008; Jorgensen et al, 2008). In contrast, other mono-ADP-RTs (e.g., the T3SE ExoS from P. aeruginosa) target numerous host proteins (Hauser, 2009). The study of mono-ADP-RT T3SEs from phytopathogenic bacteria is still in its infancy. HopU1 from Pto DC3000 was the first from this family with a proven role in virulence and targets several plant RBPs, including GRP7 and GRP8 (Fu et al, 2007). More recently, the plasma membrane-targeted T3SE mono-ADP-RT HopF2 from Pto DC3000 was also shown to target multiple plant proteins, including the MAP kinase kinase MKK5 and the important immune regulator RIN4, to suppress PTI and cause disease (Wang et al, 2010; Wilton et al, 2010; Wu et al, 2011). The T3SE HopF1/AvrPphF from P. syringae pv. phaseolicola race 7 shows weak homology to mono-ADP-RTs

and is required for virulence on bean (Tsiamis et al, 2000; Singer et al, 2004), but no corresponding host target has been identified so far.

GRP7 is required for PTI responses triggered by several PAMPs, including flg22, elf18 and chitin (Fu et al, 2007; Jeong et al, 2011). In addition, we have shown that GRP7 overexpression increases early and late PTI responses triggered by these PAMPs (Figure 1). Similarly, loss of and overexpression of GRP7 leads to reduced and increased resistance to Pto DC3000, respectively (Figure 1; Fu et al, 2007; Jeong et al, 2011). These results demonstrate that GRP7 is an important immune regulator that is both required and limiting for full immunity to Pto DC3000. Despite these findings, the exact role of GRP7 in PTI was still unclear. RBPs can be involved in different aspects of RNA metabolism (e.g., splicing, transport, storage, translation and degradation) (Keene, 2007). According to a potential role in RNA-related processes, we found that GRP7 associates in vivo specifically with several components of the translational machinery, including eIF4A1, eIF4A2, eEF1A, eIF4E and S14 (Figures 3 and 4; Supplementary Figure S7; Supplementary Table S1). The association of GRP7 with an active translational complex is further suggested by the enrichment of a slower migrating form of eIF4E in the GRP7 immunoprecipitate (Figures 3 and 4; Supplementary Figure S7), which may correspond to the phosphorylated active form of eIF4E that is linked to the mRNA cap (Beretta et al, 1998; Raught and Gingras, 1999; Dyer et al, 2003).

Unexpectedly, we also found that GRP7 directly interacts in vivo with the PRRs FLS2 and EFR in a specific manner (Figure 2; Supplementary Figure S3), as GRP7 did not interact with the LRR-RLK BAK1 (Figure 2C) that is involved in PTI signalling downstream of FLS2 and EFR (Chinchilla et al,

2007; Heese et al, 2007; Roux et al, 2011). Notably, the interaction between GRP7 and FLS2 (and EFR) appears to be at the plasma membrane, as indicated by the localization of the YFP signal in BiFC experiments (Figure 2E; Supplementary Figure S3B) and the presence of FLS2 (and EFR) in co-immunoprecipitation experiments (Figures 2A, B and D). In addition, GRP7 and GRP8 are present in highly purified A. thaliana plasma membrane preparations (Alexandersson et al, 2004). Interestingly, a potential direct and dynamic link between the GRP7–FLS2 complex and the complex between GRP7 and translational components is indicated by the flg22-induced dissociation of elF4E and S14 from the GRP7 complex (Figure 3). This observation is reminiscent of the recent demonstration in mammals and plants of transmembrane receptor-associated translational regulation complexes that most likely enable rapid activation of ligand-induced translation (Ehsan et al, 2005; Carvalho et al, 2008; Lin et al, 2010; Tcherkezian et al, 2010). Previous electron microscopy experiments revealed the presence of polysomes anchored to the plasma membrane via actin filaments in both plant and animal cells (Hovland et al, 1996; Medalia et al, 2002). Therefore, the reported association of FLS2 with translation regulation complexes at the plasma membrane is of great interest for further studies.

However, we found that HopU1 does not directly target FLS2 by mono-ADP-ribosylation (Supplementary Figure S5), nor perturb the association or the dissociation between GRP7 and FLS2 or translational components (Figure 4; Supplementary Figure S7) despite directly interacting with GRP7 (Supplementary Figure S6). These results suggest that HopU1 targets another molecular function of GRP7 that is independent of the aforementioned protein–protein interactions. In addition to the previously reported binding of GRP7 to its own transcript and that of GRP8 in vitro

(Staiger et al, 2003; Schoning et al, 2008), we found that GRP7 binds the transcripts of FLS2 and EFR in vivo, but not of BAK1 (Figure 5A; Supplementary Figure S8). As shown for its own transcript (Schoning et al, 2007), GRP7 binds the 3′-UTR of FLS2 mRNA in vitro (Figures 5B and C). To our knowledge, FLS2 and EFR correspond to the first described non-RBP cargo mRNAs bound by GRP7 and GRP8 with a clear biological function. However, it is clear that GRP7 carries other cargo mRNAs involved in immunity and other processes that require identification, as GRP7 has been also involved in circadian clock, flowering time and tolerance to abiotic stresses (Mangeon et al, 2010). An effect on these cargo mRNAs may explain some of the immune phenotypes observed in the GRP7 overexpressing lines. Importantly, however, we demonstrated that HopU1 inhibits the GRP7–FLS2 mRNA and GRP7–EFR mRNA interactions in vivo, and that these interactions depend on R49 (Figure 6; Supplementary Figure S8), the conserved residue that is mono-ADP-ribosylated by HopU1 and located within the RRM RNA-binding domain of GRP7 (Jeong et al, 2011). This is consistent with the previously reported importance of this residue for RNA binding in vitro (Schoning et al, 2007; Jeong et al, 2011). Our results provide examples of relevant immune-related target mRNAs whose binding to GRP7 is inhibited by HopU1 in vivo. Furthermore, we could show that the injection of HopU1 by the type III secretion system during Pto DC3000 infection leads to reduced FLS2 accumulation in planta (Figure 7). Notably, the effect of HopU1 on FLS2 amounts is comparable to the previously described effect of the Pto DC3000 T3SE AvrPtoB or the Arabidopsis E3 ligases PUB12/13 (Gohre et al, 2008; Lu et al, 2011). This suggests that the inability of GRP7 to bind FLS2 mRNA ultimately results in decreased FLS2 accumulation during infection, potentially by inhibiting FLS2 translation.

In apparent contradiction to our model, we only found slightly reduced

FLS2 protein levels in HopU1 A. thaliana seedlings under sterile conditions (Supplementary Figure S2C). However, we hypothesize that GRP7 is not involved in steady-state synthesis of FLS2, but rather regulates pathogen-induced FLS2 translation. Indeed, FLS2 gene expression is induced upon PAMP treatment (Zipfel et al, 2004, 2006), and FLS2 accumulates strongly upon infection with Pto DC3000 hrcC$^-$ (Figure 7A) that only triggers PTI, given its inability to secrete PTI-suppressing T3SEs. Notably, consistent with the fact that GRP7 does not bind BAK1 mRNA (Figures 5 and 6; Supplementary Figure S8), HopU1 does not affect BAK1 protein levels during infection (Supplementary Figure S10).

In accordance with our hypothesis, we observed that GRP7ox seedlings accumulate about 20% more FLS2 protein after 4 h of flg22 treatment than WT seedlings (Supplementary Figure S11). Although we could not prove that FLS2 mRNA was associated with GRP7 in complex with FLS2 at the plasma membrane, our results suggest the existence of a complex including FLS2 mRNA, GRP7, translational components and FLS2 in a plasma membrane-associated complex that may contribute to pathogen-induced de novo translation of FLS2 during the early steps of plant infection. An additional argument in favour of this hypothesis is that flg22 perception induces the release of the 43S complex from GRP7, potentially to start de novo protein synthesis. Notably, flg22 binding leads to FLS2 endocytosis and FLS2 degradation upon binding to E3 ligases (Robatzek et al, 2006; Lu et al, 2011). Therefore, it is possible that de novo pathogen-induced FLS2 translation is involved in the rapid replenishment of the plasma-membrane pool of ligand-free FLS2. In this model, HopU1 would inhibit GRP7–FLS2 mRNA interaction and thus block the recruitment of FLS2 transcripts into the plasma membrane-associated complex, leading most likely to the

inhibition of de novo pathogen-induced FLS2 translation. Further work will be needed to test this model.

During the infection process, pathogenic effectors must collaborate in a complementary manner to suppress efficiently host innate immune responses. Importantly, the secretion and action of T3SEs occur after or while PAMPs are perceived, given that the T3SS is only induced in planta (Boch et al, 2002). The T3SEs AvrPto and AvrPtoB target the FLS2 pathway by blocking the activation of FLS2 and/or BAK1, and by inducing FLS2 degradation (Xing et al, 2007; Gohre et al, 2008; Shan et al, 2008; Xiang et al, 2008, 2011; Gimenez-Ibanez et al, 2009; Cheng et al, 2011; Zeng et al, 2012). In addition, the T3SEs AvrPphB and AvrAC target the immediate substrate of the FLS2-BAK1 complex, BIK1 and related proteins, for degradation or inhibition, respectively (Zhang et al, 2010; Feng et al, 2012). In this paper, we reveal that HopU1 may have a synergic effect with previously described Pseudomonas T3SEs by inhibiting PAMP-induced de novo FLS2 synthesis, which would otherwise compensate for the negative action of AvrPto, AvrPtoB and AvrPphB on innate immunity. The importance of FLS2 as an important virulence target for HopU1 is demonstrated by the strict dependency on the presence of flagellin to observe the hypo-virulence phenotype of Pto DC3000 ΔhopU1 on WT A. thaliana plants (Figure 7D).

The demonstration that GRP7 binds PRR-encoding transcripts, and that the Pto DC3000 T3SE HopU1 inhibits this interaction in a manner dependent on its mono-ADP-RT activity ultimately leading to reduced PRR accumulation during infection, provides a first direct link between GRP7 and a function in PTI, and reveals a novel virulence mechanism employed by bacterial pathogens. This mechanism is in contrast with the virulence strategy

employed by C. diphtheriae, P. aeruginosa and V. cholerae that use their mono-ADP-RT toxins (DT, ExoA and colix toxin, respectively) to eradicate host translation via the targeting of eEF2 (Deng and Barbieri, 2008; Jorgensen et al, 2008). In addition, the virulence strategy used by HopU1 differs from strategies deployed by previously described T3SEs from phytopathogenic bacteria that target the PRR proteins themselves or the signalling triggered by PRR activation (Block and Alfano, 2011).

Materials and methods

Plant material

A. thaliana, N. benthamiana and N. tabacum were grown at 20–21°C with a 10-h-photoperiod in environmentally controlled chambers. Arabidopsis seedlings were grown on plates containing Murashige and Skoog (MS) medium (Duchefa) and 1% sucrose at 22°C with a 16-h photoperiod.

All experiments were performed in Col-0 background, except if indicated otherwise. The fls2 mutant used in this study is SALK_093905. The GRP7ox (Col-2/35S::GRP7), HopU1 (Col-0/35S::HopU1-HA), GRP7-GFP (Col-0/35S::GRP7-GFP), GRP7-HA (grp7-1/GRP7p::GRP7-HA) and GRP7(R49K)-HA [grp7-1/GRP7p::GRP7(R49K)-HA] were previously published in Fu et al (2007); Kim et al (2008); Streitner et al (2008); Jeong et al (2011). The GRP7-GFP/HopU1 line was obtained by crossing the GRP7-GFP and HopU1 lines.

The estradiol-inducible HopU1 line (ind_HopU1) was obtained by transforming Col-0 with the vector pLN604 (derived from pER8; Zuo et al, 2000) carrying hopU1-HA. The expression of HopU1 was induced by spraying 15 μM β-estradiol for 16–20 h. The GRP8-HA (Col-0/35S::GRP8-

HA) line was obtained by transforming Col-0 with the binary vector pPZP212 carrying GRP8-HA. Homozygous lines with a single transgene insertion were used for the experiments.

PTI assays

PAMP treatments (flg22 and elf18 peptides synthetized by Peptron, South Korea; shrimp chitin from SIGMA) were performed by syringe infiltration of plant leaves or by addition of the elicitor into the liquid media. Oxidative burst assays were performed on leaf disks incubated in a solution containing luminol and peroxidase as previously described (Zipfel et al, 2004). Callose deposition was observed after infiltration with a solution of 1 µM PAMP for 16 h as previously described (Hann and Rathjen, 2007). Callose deposits were quantified using PDQuest software (Bio-Rad).

Pseudomonas infection

Bacterial strains used in this study were Pseudomonas syringae pv. tomato (Pto) DC3000 WT, Pto DC3000 ΔhopU1 and Pto DC3000 hrcC$^-$. For bacterial enumeration assays, plants were sprayed with the strains WT (inoculum: 10^6 cfu/ml), ΔhopU1 (inoculum: 10^8 cfu/ml) and hrcC$^-$ (inoculum: 10^8 cfu/ml), in the presence of 0.001% (v/v) Silwet L-77. Sprayed plants were then covered with a transparent plastic lid for the remaining of the experiment. For the other assays, bacteria were infiltrated into Arabidopsis leaves with the strains WT (inoculum: 5×10^7 cfu/ml), ΔhopU1 (inoculum: 10^8 cfu/ml) and hrcC$^-$ (inoculum: 10^8 cfu/ml).

For the trans-complementation experiment described in Figure 7, pLN1981, encoding HopU1-HA, and pLN1982, encoding HopU1DD-HA, were electroporated into UNL141, the DC3000 ΔhopU1 mutant (Fu et al, 2007).

The ΔhopU1(HopU1) and ΔhopU1(HopU1DD) strains were confirmed to produce HopU1-HA and HopU1DD-HA prior to using these strains to infect Arabidopsis.

The construction of ΔfliC mutant was done by unmarked mutagenesis (House et al, 2004). A 1.9-kb upstream (US) DNA sequence and 1.5-kb downstream (DS) were amplified by PCR using the primers fliC us-F (CACCGAGGTTACATGCAACGCCTG) and fliC us-R (CATGATGAATTCCTCGTTGG) and fliC ds-F (CACCCAGTAATATCGGCATGAG) and fliC-R (CGCTGATCGAACCCTTGGTC). The purified PCR products were cloned into the pENTR/D-TOPO vector (Invitrogen). Entry constructs were then recombined by LR reactions into pMK2017 for US sequence and pMK2016 for DS sequences. These plasmids were separately introduced into DC3000 and plated onto media selecting for integration of each plasmid into DC3000 genome. Deletion of fliC was performed following a previously published protocol (Crabill et al, 2010). For construction of the fliC hopU1 double mutant, ΔfliC was used as a background strain to generate a hopU1 deletion mutation via homologous recombination using constructs described in Fu et al (2007). The resulting mutants were confirmed with PCR using primers that annealed to the flanking regions of either fliC or hopU1.

Yeast two-hybrid

The coding region corresponding to the cytoplasmic part of EFR (EFRcyt) was cloned in the pLexA vector. The recombinant pLexA-EFRcyt was used to screen a cDNA library prepared from infected Arabidopsis plants (van der Biezen et al, 2000) according to the indications of the manufacturer (LexA system-based yeast two hybrid; CLONTECH). The coding region of GRP7 from the nucleotides 67 to 528 (corresponding to the region of the GRP7

clone identified during the initial screen) was re-cloned in the pB42AD vector to retest the interaction.

Agrobacterium-mediated transient expression for co-immunoprecipitation, subcellular localization and BiFC experiments

For the co-immunoprecipitation and subcellular localization experiments, we used the following previously described constructs: 35S::GRP7-eGFP (Fu et al, 2007), 35S::EFR-3 × HA (Schwessinger et al, 2011), 35S::FLS2-3 × myc (Chinchilla et al, 2006), 35S::BAK1-HA (Schwessinger et al, 2011), 35S::FLS2-GFP-His (Schwessinger et al, 2011) and 35S::HopU1-HA (Fu et al, 2007). The Agrobacterium strains GV3101 carrying the indicated constructs were syringe-infiltrated in N. benthamiana or N. tabacum leaves at OD_{600}=0.4–0.6 and samples were collected 2 days post infiltration.

For the BiFC assays, we cloned the coding regions of FLS2, EFR, GRP7 and HopU1 into the BiFC binary vectors pAM-PAT-35S that were previously described in Lefebvre et al (2010). The Agrobacterium strain GV3101 expressing the silencing suppressor P19 (Voinnet et al, 2003) and carrying the indicated constructs were syringe-infiltrated in N. benthamiana leaves at OD_{600}=0.4–0.6.

Confocal analyses for the subcellular localization and BiFC experiments were performed 2 days post infiltration using a Leica SP5 confocal microscope.

Protein extraction, co-immunoprecipitation and immunoblotting

Total proteins were extracted in a buffer including 100 mM Tris–HCl pH 7.5, 150 mM NaCl, 5 mM EDTA, 5% glycerol, 10 mM DTT, 0.5% Triton X-100, 1% Igepal and protease inhibitors (Sigma). For co-

immunoprecipitation, anti-HA beads (Roche) or anti-GFP-TRAP-A beads (Chromotek) were incubated with total proteins and then washed with the extraction buffer. Proteins were fractioned on SDS–PAGE, transferred onto PVDF membranes (Bio-Rad) and then detected using specific antibodies. FLS2 was detected using specific polyclonal antibodies raised in rabbit as primary antisera. The anti-S14-1 antibodies were purchased (Agrisera, Sweden). The rabbit anti-eIF4E antibody was a kind gift from Professor A Maule (John Innes Centre, Norwich, UK). Epitope-tagged proteins were detected with a peroxidase-conjugated anti-HA-HRP (Santa Cruz); mouse monoclonal anti-GFP antibodies (AMS); or anti-HRP antibodies (Santa Cruz). The secondary anti-rabbit-HRP antibodies (Sigma) were used when appropriate. Immunodetection was performed with ECL chemiluminescence reagent (GE). Tandem mass-spectrometry experiments have been performed as previously described (Fu et al, 2007).

In vitro ADP-ribosylation assay

HopU1-His, GRP7-GST and FLS2-GST were affinity-purified from Escherichia coli BL21 and the purity of the proteins was examined by SDS–PAGE. The ADP-ribosylation assay was performed as previously (Fu et al, 2007).

RNA-immunoprecipitation assay

After UV-crosslinking treatments (120 MJ, 3 times using UV Stratalinker^{TM} 2400, Stratagene), total proteins were extracted in extraction buffer including 50 mM Tris–HCl pH 8, 150 mM NaCl, 2.5 mM EDTA, 10% glycerol, 10 mM PMSF, 10 units/ml RNaseOUT (Invitrogen) and protease inhibitors (Sigma). After centrifugation, the supernatant was incubated with anti-HA affinity matrix (Roche) or anti-GFP-TRAP-A beads (Chromotek).

After this incubation, the beads were washed and the RNA-GRP7 complexes were eluted by incubating at 60°C for 15 min in the elution buffer (1% SDS, 0.1 M $NaHCO_3$). A proteinase K treatment for 1 h at 60°C was then followed by RNA extraction and quantitative RT–PCR.

In each experiment, transcript levels from the input have been normalized in comparison to the control samples (grp7/GRP7-HA in Figures 5A and 6B and Supplementary Figure S7B; HopU1 in Figure 6A and Supplementary Figure S7A; and Col-0 in Supplementary Figure S8). The normalization of the transcript levels after RNA-IP has been performed in comparison to the GRP7 transcript level in grp7/GRP7-HA or GRP7-GFP samples (Figures 5A, 6A and B, Supplementary Figures S7A and B) or the GRP8 transcript level (Supplementary Figure S8).

Quantitative RT–PCR

After RNA extraction (Tri Reagent, Sigma-Aldrich), first-strand cDNA was synthesized using the SuperScript II Reverse Transcriptase (Invitrogen). Quantitative PCRs were performed from 1.5 µl of cDNA with SYBR Green JumpStart Taq ReadyMix (Sigma-Aldrich) on a PTC-200 Peltier Thermal Cycler (MJ Research, Waltham, MA). Primers used are

Ubox (At5g15400): 5′-TGCGCTGCCAGATAATACACTATT-3′ and

5′-TGCTGCCCAACATCAGGTT-3′

FLS2 (At5g46330): 5′-ACTCTCCTCCAGGGGCTAAGGAT-3′ and

5′-AGCTAACAGCTCTCCAGGGATGG-3′

EFR (At5g20480): 5′-CGGATGAAGCAGTACGAGAA-3′ and

5′-CCATTCCTGAGGAGAACTTTG-3′

BAK1 (At4g33430): 5′-ACCGCCTCCTATCTCTCCTACACC-3′ and

5′-CTGGGTCCTCTTCAGCTGGTACA-3′

GRP7 (At2g21660): 5′-TGATGACAGAGCTCTTGAGACTGCC-3′ and

5′-TCCTCCTCCACCCTCGCGTCTACCGCCGCCA-3′

GRP8 (At4g39260): 5′-CAATGATGAAGATCTTCAAAGGACG-3′ and

5′-CTCGTAACCACCACCGCCTCCTCCTGAGTATCC-3′

Electrophoretic mobility shift assay

The 3'-UTR sequence of FLS2 was amplified with the upstream primer GATGGTACCGAAGTTTAGCAGCAAAGC and the downstream primer GAGCTCGAGGTTCATCAAAACCAAATTTC. The amplified fragment was subcloned into the plasmid pBSK(-) (Stratagene) and transcribed with T7 polymerase (Promega) in the presence of 10 µCi ^{32}P CTP. The FLS2 3′-UTR binding affinity was analysed with purified GRP7-GST in 20 mM HEPES, pH 7.5, 100 mM NaCl, 1 mM $MgCl_2$, 0.01% NP-40, 10 U SUPERase·In (Ambion), and 50 ng of ^{32}P-labelled FLS2 3′-UTR. Inhibition of RNA binding ability by HopU1 was tested by first producing mono-ADP-ribosylated GRP7, then performing an electrophoretic mobility shift assay. Four µM GRP7-GST was incubated with 1 µM HopU1-His or HopU1DD-His in the standard ADP-ribosylation reaction followed by analysis of RNA binding ability. For competition assays, unlabelled FLS2 3'-UTR transcripts were added into the mixture of 2 µM GRP7-GST and 50 ng of ^{32}P-labelled FLS2 3′-UTR transcripts. The bound and free RNA probes were separated

on 6% native PAGE and exposed to PhotoImage screen, then analysed by Storm 860 scanner (Molecular Dynamics).

Statistical analysis

Statistical significances based on one-way ANOVA were performed with Prism 5.01 software (GraphPad Software).

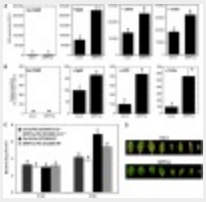

View larger version

Figure 1. GRP7 overexpression enhances significantly PTI responses and resistance to *Pseudomonas* infection. (**A**) Oxidative burst triggered by 1 µM flg22, 1 µM elf18, 100 µg/ml chitin or in absence of PAMP treatment in Col-2 and transgenic *A. thaliana* plants overexpressing GRP7 (GRP7ox). ROS production is presented as total photon count during 25 min of treatment and measured in relative light units (RLUs). Values are mean±s.e. (*n*=6). Statistical significance was assessed using the ANOVA test (*P*<0.001). (**B**) Callose deposition induced by 1 µM flg22, 1 µM elf18, 100 µg/ml chitin or in absence of PAMP treatment, directly infiltrated in Col-2 and transgenic *A. thaliana* plants overexpressing GRP7 (GRP7ox). Values are mean±s.e. (*n*=24). Statistical significance was assessed using the ANOVA test (*P*<0.001). ND, non-detectable. (**C**) Growth of *Pseudomonas syringae* pv. *tomato* (*Pto*) DC3000 on Col-2 and GRP7ox plants as measured by colony forming units (cfu). Bacterial growth was measured 4 days after spray inoculation with the wild-type strain (WT) or the *hrcC*$^{-}$ strain. Values are mean±s.e. (*n*=4). dai, days after inoculation. Statistical significance was assessed using the ANOVA test (*P*<0.001; letters indicate statistically significant differences). (**D**) Disease symptoms on Col-2 and GRP7ox plants, 4 days after spray infection with *Pto* DC3000 WT. All results shown are representative of at least three independent experiments.

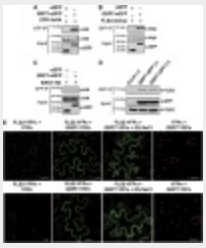

View larger version

Figure 2. GRP7 associates with FLS2 at the plasma membrane. (**A**–**C**) Co-immunoprecipitation assay performed after transient co-expression of GRP7-eGFP or eGFP with EFR-3 × HA (**A**), FLS2-3 × myc (**B**) or BAK1-HA (**C**) in *N. benthamiana* plants. Total proteins (input) were subjected to immunoprecipitation with GFP Trap beads followed by immunoblot analysis. (**D**) Co-immunoprecipitation of GRP7 and FLS2 in *A. thaliana*. Co-immunoprecipitation assay performed on Col-0 and GRP7-GFP plants untreated (−) or treated (+) with 1 µM flg22 for 15 min. Total proteins (input) were subjected to immunoprecipitation with GFP Trap beads followed by immunoblot analysis. (**E**) Bimolecular fluorescence complementation assays between GRP7 and FLS2. YFPn, GRP7-YFPn, YFPc and FLS2-YFPc, as well as the reverse combinations YFPc, GRP7-YFPc, YFPn and FLS2-YFPn, were transiently co-expressed in *N. benthamiana* leaves. Plasmolysis experiment was performed in the presence of 5% NaCl for 5 min. Arrows indicate Hechtian strands. The chlorophyll autofluorescence appears in red. Scale bar corresponds to 20 µm. Photographs were taken 2 days after infiltration and are representative of the total observations (*n*=60). All results shown are representative of three independent experiments.

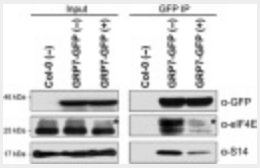

View larger version

Figure 3. GRP7 associates with translational components in *Arabidopsis*. Co-immunoprecipitation of GRP7 and translational components in *A. thaliana*. Co-immunoprecipitation assay performed on Col-0 and GRP7-GFP plants untreated (−) or treated (+) with 1 µM flg22 for 15 min. Total proteins (input) were subjected to immunoprecipitation with GFP Trap beads followed by immunoblot analysis with anti-GFP antibodies to detect GRP7-GFP or specific antibodies recognizing the translation initiation factor eIF4E and the ribosomal protein S14. Asterisks mark eIF4E slower migrating bands. The results shown are representative of three independent experiments.

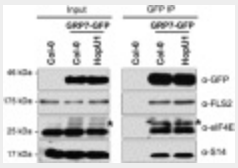

View larger version

Figure 4. HopU1 does not affect the protein–protein interactions between GRP7, FLS2 and translational components. Co-immunoprecipitation of GRP7-associated proteins in the presence of HopU1 in *A. thaliana*. Co-immunoprecipitation assay performed on Col-0 and HopU1 plants expressing or not GRP7-GFP. Total proteins (input) were subjected to immunoprecipitation with GFP Trap beads followed by immunoblot analysis with anti-GFP antibodies to detect GRP7 or specific antibodies recognizing FLS2, the translation initiation factor eIF4E, or the ribosomal protein S14. Asterisks mark slower migrating band forms. The results shown are representative of three independent experiments.

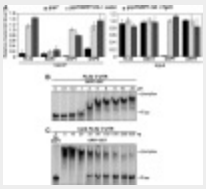

View larger version

Figure 5. GRP7 binds *FLS2* transcript. (**A**) RNA immunoprecipitation in *grp7-1* and *grp7-1*/GRP7-HA *A. thaliana* lines treated for 30 min with water or 1 µM flg22. Total proteins were subjected to immunoprecipitation with anti-HA antibodies followed by quantitative RT–PCR analysis of *FLS2*, *BAK1*, *GRP7* and *GRP8* transcripts with specific primers. Values are mean±s.e. (*n*=4). The results shown are representative of three independent experiments. (**B**, **C**) GRP7 binds the 3′UTR of *FLS2* transcripts *in vitro*. Electrophoretic shift assays performed on the 3′UTR of *FLS2* RNAs, in presence of increasing concentrations of GRP7-GST (**B**). Competition assay was performed with increasing quantity of unlabelled *FLS2* 3′UTR transcripts to GRP7-GST and ^{32}P-labelled *FLS2* 3'UTR transcripts (**C**). The results shown are representative of three independent experiments.

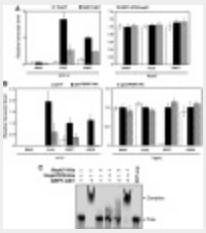

View larger version

Figure 6. HopU1 disrupts GRP7–*FLS2* transcripts interactions. (**A**) RNA immunoprecipitation in HopU1, GRP7-GFP and GRP7-GFP/HopU1 *A. thaliana* lines. Total proteins were subjected to immunoprecipitation with GFP Trap beads followed by quantitative RT–PCR analysis of *BAK1*, *FLS2* and *GRP7* transcripts with specific primers. Values are mean±s.e. (*n*=4). (**B**) RNA immunoprecipitation in *grp7*, *grp7/*GRP7-HA and *grp7/*GRP7(R49K)-HA *A. thaliana* lines. Total proteins were subjected to immunoprecipitation with anti-HA matrix beads followed by quantitative RT–PCR analysis of *BAK1*, *FLS2*, *GRP7* and *GRP8* transcripts with specific primers. Values are mean±s.e. (*n*=4). (**C**) Electrophoretic shift assays in the presence of HopU1 and its inactive version HopU1DD. Standard ADP-ribosylation reaction was performed with 4 μM GRP7-GST in the presence of 1 μM HopU1 or HopU1DD. The corresponding GRP7-GST was then added to the 3′-UTR of *FLS2* transcript binding assay. The results shown are representative of three independent experiments.

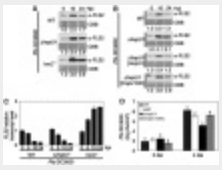

View larger version

Figure 7. HopU1 inhibits FLS2 protein accumulation during infection. (**A**) Immunoblots with specific antibodies detecting endogenous FLS2 in Col-0 during bacterial infection after syringe inoculation with *Pto* DC3000 (WT; inoculum: 5×10^7 cfu/ml), *Pto* DC3000 Δ*hopU1* (inoculum: 10^8 cfu/ml), *Pto* DC3000 *hrcC*$^-$ (inoculum: 10^8 cfu/ml). hpi, hours post infection; CBB, Coomassie Brilliant Blue. Values correspond to signal intensity of the FLS2-specific band from the immunoblots relative to the zero time point. (**B**) Immunoblots with specific antibodies detecting endogenous FLS2 in Col-0 during bacterial infection after syringe inoculation with *Pto* DC3000 (WT; inoculum: 5×10^7 cfu/ml), *Pto* DC3000 Δ*hopU1* (inoculum: 10^8 cfu/ml), *Pto* DC3000 Δ*hopU1* [HopU1] (inoculum: 10^8 cfu/ml), *Pto* DC3000 Δ*hopU1* [HopU1DD] (inoculum: 10^8 cfu/ml). hpi, hours post infection; CBB, Coomassie Brilliant Blue. Values correspond to signal intensity of the FLS2-specific band from the immunoblots relative to the zero time point. (**C**) *FLS2* transcript level as measured by quantitative RT–PCR in Col-0 plants during bacterial infection after syringe inoculation with *Pto* DC3000 (WT; inoculum: 5×10^7 cfu/ml), *Pto* DC3000 Δ*hopU1* (inoculum: 10^8 cfu/ml), *Pto* DC3000 *hrcC*$^-$ (inoculum: 10^8 cfu/ml). hpi, hours post infection. (**D**) Bacterial growth measured during *Pseudomonas* infection in Col-0 plants, after spray inoculation (inoculum: 2×10^8 cfu/ml) with *Pto* DC3000 wild-type (WT) or the derivated strains Δ*fliC*, Δ*hopU1* and Δ*hopU1*Δ*fliC*. Growth measured by colony forming units (cfu) 4 days after inoculation. Values are mean±s.e. (n=4). Statistical significance was assessed using the ANOVA test (P<0.001; letters indicate statistically significant differences). dai, days after inoculation. The results shown are representative of three independent experiments.

Supplementary Material

Open In Web Browser

Acknowledgments

We thank H Kang, A Maule and J Rathjen for sharing biological materials; F Liu and C Dean for sharing their RNA-immunoprecipitation assay protocol; J Rathjen, JDG Jones, S Robatzek and all the members of the CZ and JRA laboratories for fruitful discussions and comments on the manuscript.

Author contributions: VN, AJ, BJ, CK, FB and IW performed experiments; VN, AJ, BJ, FB, DS, JRA and CZ designed experiments and analysed the data; VN, AJ, JRA and CZ wrote the manuscript. All authors commented on the manuscript.

Footnotes

The authors declare that they have no conflict of interest.

References

- Alexandersson E, Saalbach G, Larsson C, Kjellbom P (2004) Arabidopsis plasma membrane proteomics identifies components of transport, signal transduction and membrane trafficking. Plant Cell Physiol 45: 1543–155615574830
- Beretta L, Singer NG, Hinderer R, Gingras AC, Richardson B, Hanash SM, Sonenberg N

(1998) Differential regulation of translation and eIF4E phosphorylation during human thymocyte maturation. J Immunol 160: 3269–32739531283

- Block A, Alfano JR (2011) Plant targets for Pseudomonas syringae type III effectors: virulence targets or guarded decoys? Curr Opin Microbiol 14: 39–4621227738
- Boch J, Joardar V, Gao L, Robertson TL, Lim M, Kunkel BN (2002) Identification of Pseudomonas syringae pv. tomato genes induced during infection of Arabidopsis thaliana. Mol Microbiol 44: 73–8811967070
- Carvalho CM, Santos AA, Pires SR, Rocha CS, Saraiva DI, Machado JP, Mattos EC, Fietto LG, Fontes EP (2008) Regulated nuclear trafficking of rpL10A mediated by NIK1 represents a defense strategy of plant cells against virus. PLoS Pathog 4: e100024719112492
- Cheng W, Munkvold KR, Gao H, Mathieu J, Schwizer S, Wang S, Yan YB, Wang J, Martin GB, Chai J (2011) Structural analysis of Pseudomonas syringae AvrPtoB bound to host BAK1 reveals two similar kinase-interacting domains in a Type III effector. Cell Host Microbe 10: 616–62622169508
- Chinchilla D, Bauer Z, Regenass M, Boller T, Felix G (2006) The Arabidopsis receptor kinase FLS2 binds flg22 and determines the specificity of flagellin perception. Plant Cell 18: 465–47616377758
- Chinchilla D, Zipfel C, Robatzek S, Kemmerling B, Nurnberger T, Jones JD, Felix G, Boller T (2007) A flagellin-induced complex of the receptor FLS2 and BAK1 initiates plant defence. Nature 448: 497–50017625569
- Crabill E, Joe A, Block A, van Rooyen JM, Alfano JR (2010) Plant immunity directly or indirectly restricts the injection of type III effectors by the Pseudomonas syringae type III secretion system. Plant Physiol 154: 233–24420624999
- Deng Q, Barbieri JT (2008) Molecular mechanisms of the cytotoxicity of ADP-ribosylating toxins. Annu Rev Microbiol 62: 271–28818785839
- Dodds PN, Rathjen JP (2010) Plant immunity: towards an integrated view of plant-pathogen interactions. Nat Rev Genet 11: 539–54820585331
- Dyer JR, Michel S, Lee W, Castellucci VF, Wayne NL, Sossin WS (2003) An activity-dependent switch to cap-independent translation triggered by eIF4E dephosphorylation. Nat Neurosci 6: 219–22012592407
- Ehsan H, Ray WK, Phinney B, Wang X, Huber SC, Clouse SD (2005) Interaction of Arabidopsis BRASSINOSTEROID-INSENSITIVE 1 receptor kinase with a homolog of mammalian TGF-beta receptor interacting protein. Plant J 43: 251–26115998311
- Feng F, Yang F, Rong W, Wu X, Zhang J, Chen S, He C, Zhou JM (2012) A Xanthomonas

uridine 5′-monophosphate transferase inhibits plant immune kinases. Nature 485: 114–11822504181

- Fu ZQ, Guo M, Jeong BR, Tian F, Elthon TE, Cerny RL, Staiger D, Alfano JR (2007) A type III effector ADP-ribosylates RNA-binding proteins and quells plant immunity. Nature 447: 284–28817450127
- Gimenez-Ibanez S, Hann DR, Ntoukakis V, Petutschnig E, Lipka V, Rathjen JP (2009) AvrPtoB targets the LysM receptor kinase CERK1 to promote bacterial virulence on plants. Curr Biol 19: 423–42919249211
- Gohre V, Spallek T, Haweker H, Mersmann S, Mentzel T, Boller T, de Torres M, Mansfield JW, Robatzek S (2008) Plant pattern-recognition receptor FLS2 is directed for degradation by the bacterial ubiquitin ligase AvrPtoB. Curr Biol 18: 1824–183219062288
- Gomez-Gomez L, Boller T (2000) FLS2: an LRR receptor-like kinase involved in the perception of the bacterial elicitor flagellin in Arabidopsis. Mol Cell 5: 1003–101110911994
- Hann DR, Rathjen JP (2007) Early events in the pathogenicity of Pseudomonas syringae on Nicotiana benthamiana. Plant J 49: 607–61817217460
- Hauser AR (2009) The type III secretion system of Pseudomonas aeruginosa: infection by injection. Nat Rev Microbiol 7: 654–66519680249
- Haweker H, Rips S, Koiwa H, Salomon S, Saijo Y, Chinchilla D, Robatzek S, von Schaewen A (2010) Pattern recognition receptors require N-glycosylation to mediate plant immunity. J Biol Chem 285: 4629–463620007973
- Heese A, Hann DR, Gimenez-Ibanez S, Jones A, He K, Li J, Schroeder JI, Peck SC, Rathjen JP (2007) The receptor-like kinase SERK3/BAK1 is a central regulator of innate immunity in plants. Proc Natl Acad Sci USA 104: 12217–1222217626179
- House BL, Mortimer MW, Kahn ML (2004) New recombination methods for Sinorhizobium meliloti genetics. Appl Environ Microbiol 70: 2806–281515128536
- Hovland R, Hesketh JE, Pryme IF (1996) The compartmentalization of protein synthesis: importance of cytoskeleton and role in mRNA targeting. Int J Biochem Cell Biol 28: 1089–11058930133
- Jeong BR, Lin Y, Joe A, Guo M, Korneli C, Yang H, Wang P, Yu M, Cerny RL, Staiger D, Alfano JR, Xu Y (2011) Structure function analysis of an ADP-ribosyltransferase Type III effector and its RNA-binding target in plant immunity. J Biol Chem 286: 43272–4328122013065
- Jorgensen R, Wang Y, Visschedyk D, Merrill AR (2008) The nature and character of the transition state for the ADP-ribosyltransferase reaction. EMBO Rep 9: 802–80918583986

- Keene JD (2007) RNA regulons: coordination of post-transcriptional events. Nat Rev Genet 8: 533–54317572691
- Kim JS, Jung HJ, Lee HJ, Kim KA, Goh CH, Woo Y, Oh SH, Han YS, Kang H (2008) Glycine-rich RNA-binding protein 7 affects abiotic stress responses by regulating stomata opening and closing in Arabidopsis thaliana. Plant J 55: 455–46618410480
- Lefebvre B, Timmers T, Mbengue M, Moreau S, Herve C, Tóth K, Bittencourt-Silvestre J, Klaus D, Deslandes L, Godiard L, Murray JD, Udvardi MK, Raffaele S, Mongrand S, Cullimore J, Gamas P, Niebel A, Ott T (2010) A remorin protein interacts with symbiotic receptors and regulates bacterial infection. Proc Natl Acad Sci USA 107: 2343–234820133878
- Lin KW, Yakymovych I, Jia M, Yakymovych M, Souchelnytskyi S (2010) Phosphorylation of eEF1A1 at Ser300 by TbetaR-I results in inhibition of mRNA translation. Curr Biol 20: 1615–162520832312
- Lu D, Lin W, Gao X, Wu S, Cheng C, Avila J, Heese A, Devarenne TP, He P, Shan L (2011) Direct ubiquitination of pattern recognition receptor FLS2 attenuates plant innate immunity. Science 332: 1439–144221680842
- Lummer M, Humpert F, Steuwe C, Caesar K, Schüttpelz M, Sauer M, Staiger D (2011) Reversible photoswitchable DRONPA-s monitors nucleocytoplasmic transport of an RNA-binding protein in transgenic plants. Traffic 12: 693–70221453442
- Mangeon A, Junqueira RM, Sachetto-Martins G (2010) Functional diversity of the plant glycine-rich proteins superfamily. Plant Signal Behav 5: 99–10420009520
- Medalia O, Weber I, Frangakis AS, Nicastro D, Gerisch G, Baumeister W (2002) Macromolecular architecture in eukaryotic cells visualized by cryoelectron tomography. Science 298: 1209–121312424373
- Miya A, Albert P, Shinya T, Desaki Y, Ichimura K, Shirasu K, Narusaka Y, Kawakami N, Kaku H, Shibuya N (2007) CERK1, a LysM receptor kinase, is essential for chitin elicitor signaling in Arabidopsis. Proc Natl Acad Sci USA 104: 19613–1961818042724
- Nekrasov V, Li J, Batoux M, Roux M, Chu ZH, Lacombe S, Rougon A, Bittel P, Kiss-Papp M, Chinchilla D, van Esse HP, Jorda L, Schwessinger B, Nicaise V, Thomma BP, Molina A, Jones JD, Zipfel C (2009) Control of the pattern-recognition receptor EFR by an ER protein complex in plant immunity. EMBO J 28: 3428–343819763086
- Pestova TV, Kolupaeva VG, Lomakin IB, Pilipenko EV, Shatsky IN, Agol VI, Hellen CU (2001) Molecular mechanisms of translation initiation in eukaryotes. Proc Natl Acad Sci USA 98: 7029–703611416183

- Raught B, Gingras AC (1999) eIF4E activity is regulated at multiple levels. Int J Biochem Cell Biol 31: 43–5710216943
- Robatzek S, Chinchilla D, Boller T (2006) Ligand-induced endocytosis of the pattern recognition receptor FLS2 in Arabidopsis. Genes Dev 20: 537–54216510871
- Roux M, Schwessinger B, Albrecht C, Chinchilla D, Jones A, Holton N, Malinovsky FG, Tör M, de Vries S, Zipfel C (2011) The Arabidopsis leucine-rich repeat receptor-like kinases BAK1/SERK3 and BKK1/SERK4 are required for innate immunity to hemibiotrophic and biotrophic pathogens. Plant Cell 23: 2440–245521693696
- Schoning JC, Streitner C, Meyer IM, Gao Y, Staiger D (2008) Reciprocal regulation of glycine-rich RNA-binding proteins via an interlocked feedback loop coupling alternative splicing to nonsense-mediated decay in Arabidopsis. Nucleic Acids Res 36: 6977–698718987006
- Schoning JC, Streitner C, Page DR, Hennig S, Uchida K, Wolf E, Furuya M, Staiger D (2007) Auto-regulation of the circadian slave oscillator component AtGRP7 and regulation of its targets is impaired by a single RNA recognition motif point mutation. Plant J 52: 1119–113017924945
- Schwessinger B, Roux M, Kadota Y, Ntoukakis V, Sklenar J, Jones A, Zipfel C (2011) Phosphorylation-dependent differential regulation of plant growth, cell death, and innate immunity by the regulatory receptor-like kinase BAK1. PLoS Genet 7: e100204621593986
- Segonzac C, Zipfel C (2011) Activation of plant pattern-recognition receptors by bacteria. Curr Opin Microbiol 14: 54–6121215683
- Shan L, He P, Li J, Heese A, Peck SC, Nürnberger T, Martin GB, Sheen J (2008) Bacterial effectors target the common signaling partner BAK1 to disrupt multiple MAMP receptor-signaling complexes and impede plant immunity. Cell Host Microbe 17: 17–2718621007
- Singer AU, Desveaux D, Betts L, Chang JH, Nimchuk Z, Grant SR, Dangl JL, Sondek J (2004) Crystal structures of the type III effector protein AvrPphF and its chaperone reveal residues required for plant pathogenesis. Structure 12: 1669–168115341731
- Staiger D, Zecca L, Wieczorek KDA, Apel K, Eckstein L (2003) The circadian clock regulated RNA-binding protein AtGRP7 autoregulates its expression by influencing alternative splicing of its own pre-mRNA. Plant J 33: 361–37112535349
- Streitner C, Danisman S, Wehrle F, Schoning JC, Alfano JR, Staiger D (2008) The small glycine-rich RNA binding protein AtGRP7 promotes floral transition in Arabidopsis thaliana. Plant J 56: 239–25018573194
- Tcherkezian J, Brittis PA, Thomas F, Roux PP, Flanagan JG (2010) Transmembrane receptor

DCC associates with protein synthesis machinery and regulates translation. Cell 141: 632–64420434207

- Tsiamis G, Mansfield JW, Hockenhull R, Jackson RW, Sesma A, Athanassopoulos E, Bennett MA, Stevens C, Vivian A, Taylor JD, Murillo J (2000) Cultivar-specific avirulence and virulence functions assigned to avrPphF in Pseudomonas syringae pv. phaseolicola, the cause of bean halo-blight disease. EMBO J 19: 3204–321410880434
- van der Biezen EA, Sun J, Coleman MJ, Bibb MJ, Jones JD (2000) Arabidopsis RelA/SpoT homologs implicate (p)ppGpp in plant signaling. Proc Natl Acad Sci USA 97: 3747–375210725385
- Voinnet O, Rivas S, Mestre P, Baulcombe D (2003) An enhanced transient expression system in plants based on suppression of gene silencing by the p19 protein of tomato bushy stunt virus. Plant J 33: 949–95612609035
- Wan J, Zhang XC, Neece D, Ramonell KM, Clough S, Kim SY, Stacey MG, Stacey G (2008) A LysM receptor-like kinase plays a critical role in chitin signaling and fungal resistance in Arabidopsis. Plant Cell 20: 471–48118263776
- Wang Y, Li J, Hou S, Wang X, Li Y, Ren D, Chen S, Tang X, Zhou JM (2010) A Pseudomonas syringae ADP-ribosyltransferase inhibits Arabidopsis mitogen-activated protein kinase kinases. Plant Cell 22: 2033–204420571112
- Willmann R, Lajunen HM, Erbs G, Newman MA, Kolb D, Tsuda K, Katagiri F, Fliegmann J, Bono JJ, Cullimore JV, Jehle AK, Götz F, Kulik A, Molinaro A, Lipka V, Gust AA, Nürnberger T (2011) Arabidopsis lysine-motif proteins LYM1 LYM3 CERK1 mediate bacterial peptidoclycan sensing and immunity to bacterial infection. Proc Natl Acad USA 108: 19824–19829
- Wilton M, Subramaniam R, Elmore J, Felsensteiner C, Coaker G, Desveaux D (2010) The type III effector HopF2Pto targets Arabidopsis RIN4 protein to promote Pseudomonas syringae virulence. Proc Natl Acad Sci USA 107: 2349–235420133879
- Wu S, Lu D, Kabbage M, Wei HL, Swingle B, Records AR, Dickman M, He P, Shan L (2011) Bacterial effector HopF2 suppresses Arabidopsis innate immunity at the plasma membrane. Mol Plant Microbe Interact 24: 585–59321198360
- Xiang T, Zong N, Zhang J, Chen J, Chen M, Zhou JM (2011) BAK1 is not a target of the Pseudomonas syringae effector AvrPto. Mol Plant Microbe Interact 24: 100–10720923364
- Xiang T, Zong N, Zou Y, Wu Y, Zhang J, Xing W, Li Y, Tang X, Zhu L, Chai J, Zhou JM (2008) Pseudomonas syringae effector AvrPto blocks innate immunity by targeting receptor kinases. Curr Biol 18: 74–8018158241

- Xing W, Zou Y, Liu Q, Liu J, Luo X, Huang Q, Chen S, Zhu L, Bi R, Hao Q, Wu JW, Zhou JM, Chai J (2007) The structural basis for activation of plant immunity by bacterial effector protein AvrPto. Nature 449: 243–24717694048
- Zeng L, Velasquez AC, Munkvold KR, Zhang J, Martin GB (2012) A tomato LysM receptor-like kinase promotes immunity and its kinase activity is inhibited by AvrPtoB. Plant J 69: 92–10321880077
- Zhang J, Li W, Xiang T, Liu Z, Laluk K, Ding X, Zou Y, Gao M, Zhang X, Chen S, Mengiste T, Zhang Y, Zhou JM (2010) Receptor-like cytoplasmic kinases integrate signaling from multiple plant immune receptors and are targeted by a Pseudomonas syringae effector. Cell Host Microbe 7: 290–30120413097
- Ziemienowicz A, Haasen D, Staiger D, Merkle T (2003) Arabidopsis transportin 1 is the nuclear import receptor for the circadian clock-regulated RNA-binding protein AtGRP7. Plant Mol Biol 53: 201–21214756317
- Zipfel C, Kunze G, Chinchilla D, Caniard A, Jones JD, Boller T, Felix G (2006) Perception of the bacterial PAMP EF-Tu by the receptor EFR restricts Agrobacterium-mediated transformation. Cell 125: 749–76016713565
- Zipfel C, Robatzek S, Navarro L, Oakeley EJ, Jones JD, Felix G, Boller T (2004) Bacterial disease resistance in Arabidopsis through flagellin perception. Nature 428: 764–76715085136
- Zuo J, Niu QW, Chua NH (2000) An estrogen receptor-based transactivator XVE mediates highly inducible gene expression in transgenic plants. Plant J 24: 265–27311069700

[Back]

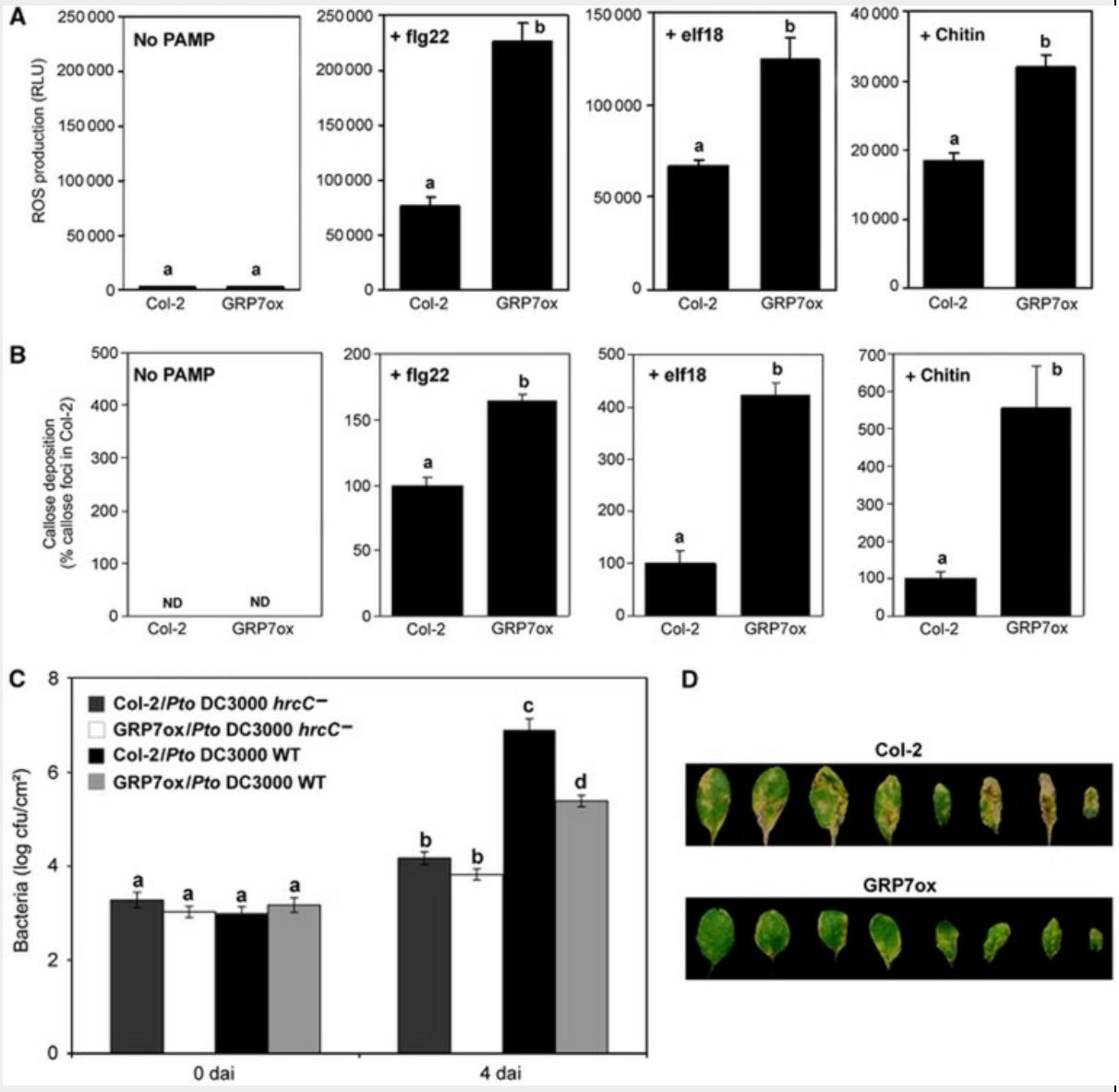

Figure 1.

GRP7 overexpression enhances significantly PTI responses and resistance to *Pseudomonas* infection. (**A**) Oxidative burst triggered by 1 µM flg22, 1 µM elf18, 100 µg/ml chitin or in absence of PAMP treatment in Col-2 and transgenic *A. thaliana* plants overexpressing GRP7 (GRP7ox). ROS production is presented as total photon count during 25 min of treatment and measured in relative light units (RLUs). Values are mean±s.e. (*n*=6). Statistical significance was assessed using the ANOVA test (*P*<0.001). (**B**) Callose deposition induced by 1 µM flg22, 1 µM elf18, 100 µg/ml chitin or in absence of PAMP treatment, directly infiltrated in Col-2 and transgenic *A. thaliana* plants overexpressing GRP7 (GRP7ox). Values are mean

±s.e. (*n*=24). Statistical significance was assessed using the ANOVA test (*P*<0.001). ND, non-detectable. (**C**) Growth of *Pseudomonas syringae* pv. *tomato* (*Pto*) DC3000 on Col-2 and GRP7ox plants as measured by colony forming units (cfu). Bacterial growth was measured 4 days after spray inoculation with the wild-type strain (WT) or the *hrcC*$^{-}$ strain. Values are mean±s.e. (*n*=4). dai, days after inoculation. Statistical significance was assessed using the ANOVA test (*P*<0.001; letters indicate statistically significant differences). (**D**) Disease symptoms on Col-2 and GRP7ox plants, 4 days after spray infection with *Pto* DC3000 WT. All results shown are representative of at least three independent experiments.

[Back]

[Back]

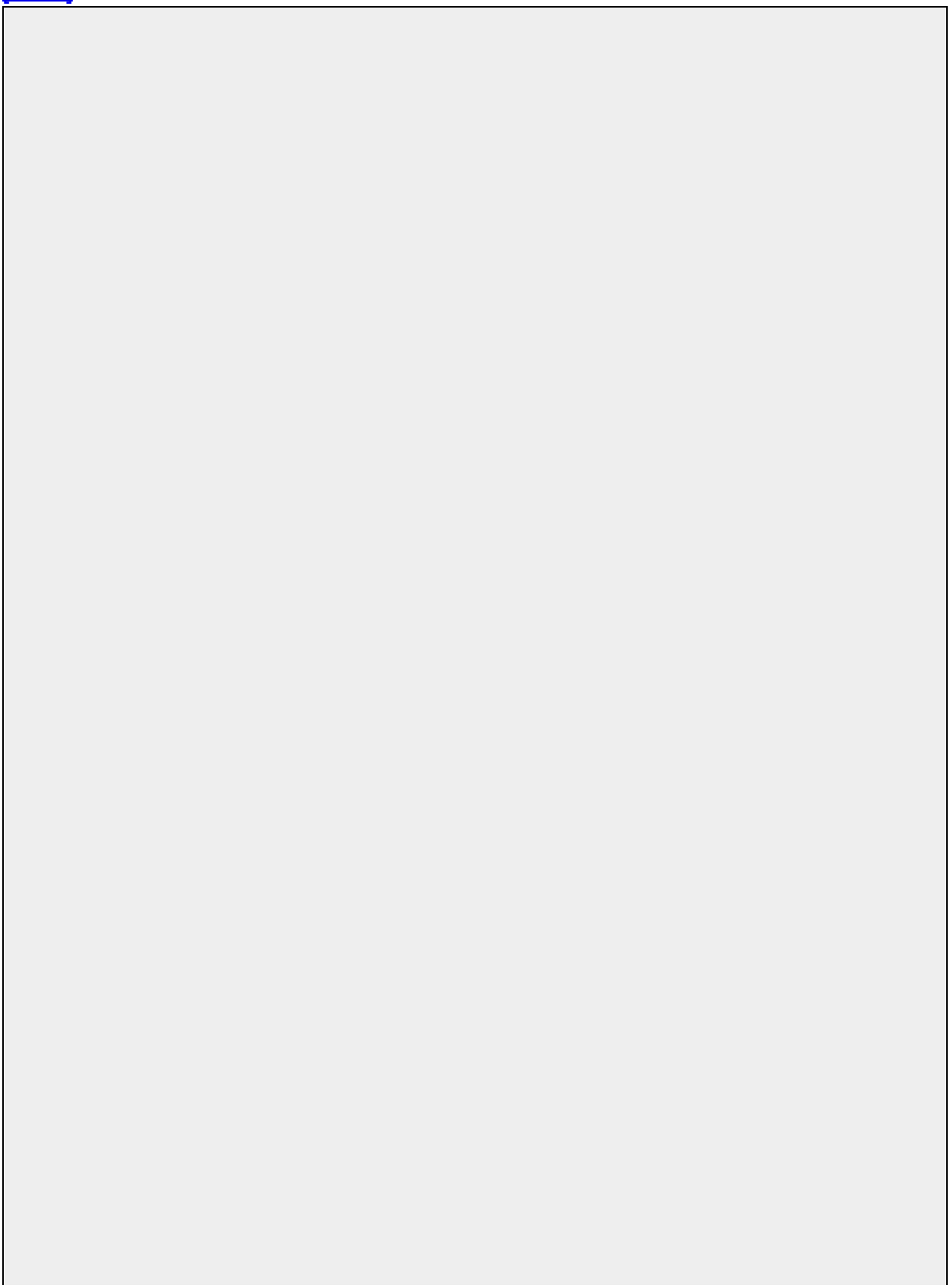

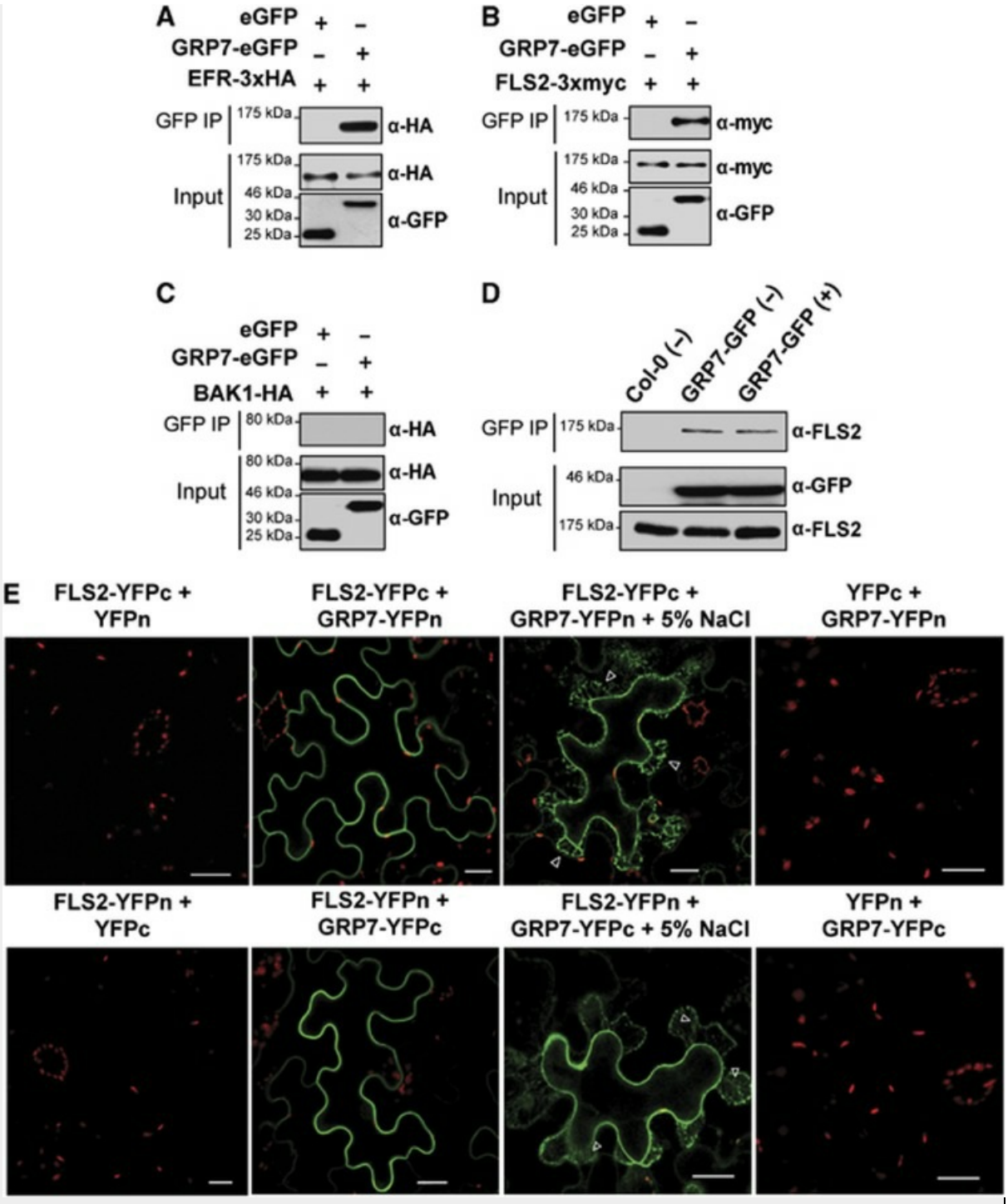

Figure 2.

GRP7 associates with FLS2 at the plasma membrane. (**A**–**C**) Co-immunoprecipitation assay performed after transient co-expression of GRP7-eGFP or eGFP with EFR-3 × HA (**A**), FLS2-3 × myc (**B**) or BAK1-HA (**C**) in *N. benthamiana* plants. Total proteins (input) were subjected to immunoprecipitation

with GFP Trap beads followed by immunoblot analysis. (**D**) Co-immunoprecipitation of GRP7 and FLS2 in *A. thaliana*. Co-immunoprecipitation assay performed on Col-0 and GRP7-GFP plants untreated (−) or treated (+) with 1 µM flg22 for 15 min. Total proteins (input) were subjected to immunoprecipitation with GFP Trap beads followed by immunoblot analysis. (**E**) Bimolecular fluorescence complementation assays between GRP7 and FLS2. YFPn, GRP7-YFPn, YFPc and FLS2-YFPc, as well as the reverse combinations YFPc, GRP7-YFPc, YFPn and FLS2-YFPn, were transiently co-expressed in *N. benthamiana* leaves. Plasmolysis experiment was performed in the presence of 5% NaCl for 5 min. Arrows indicate Hechtian strands. The chlorophyll autofluorescence appears in red. Scale bar corresponds to 20 µm. Photographs were taken 2 days after infiltration and are representative of the total observations (*n*=60). All results shown are representative of three independent experiments.

[Back]

[Back]

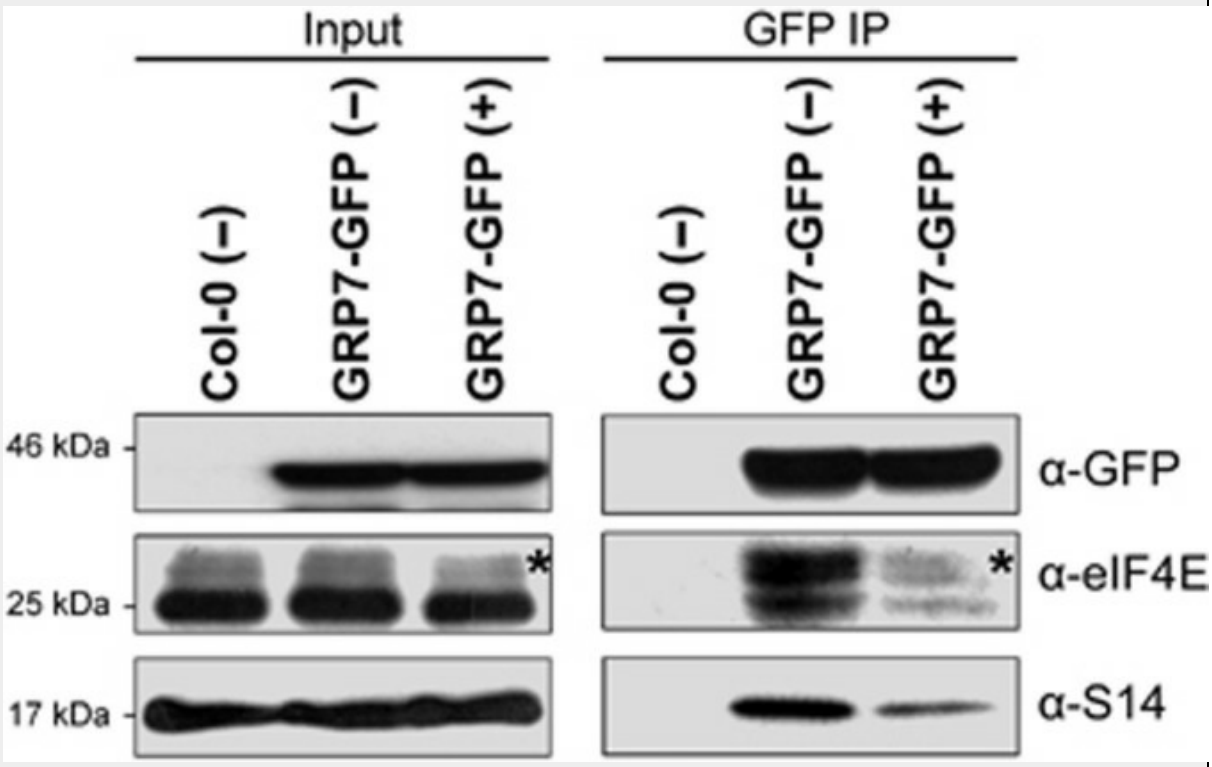

Figure 3.

GRP7 associates with translational components in *Arabidopsis*. Co-immunoprecipitation of GRP7 and translational components in *A. thaliana*. Co-immunoprecipitation assay performed on Col-0 and GRP7-GFP plants untreated (−) or treated (+) with 1 μM flg22 for 15 min. Total proteins (input) were subjected to immunoprecipitation with GFP Trap beads followed by immunoblot analysis with anti-GFP antibodies to detect GRP7-GFP or specific antibodies recognizing the translation initiation factor eIF4E and the ribosomal protein S14. Asterisks mark eIF4E slower migrating bands. The results shown are representative of three independent experiments.

[Back]

[Back]

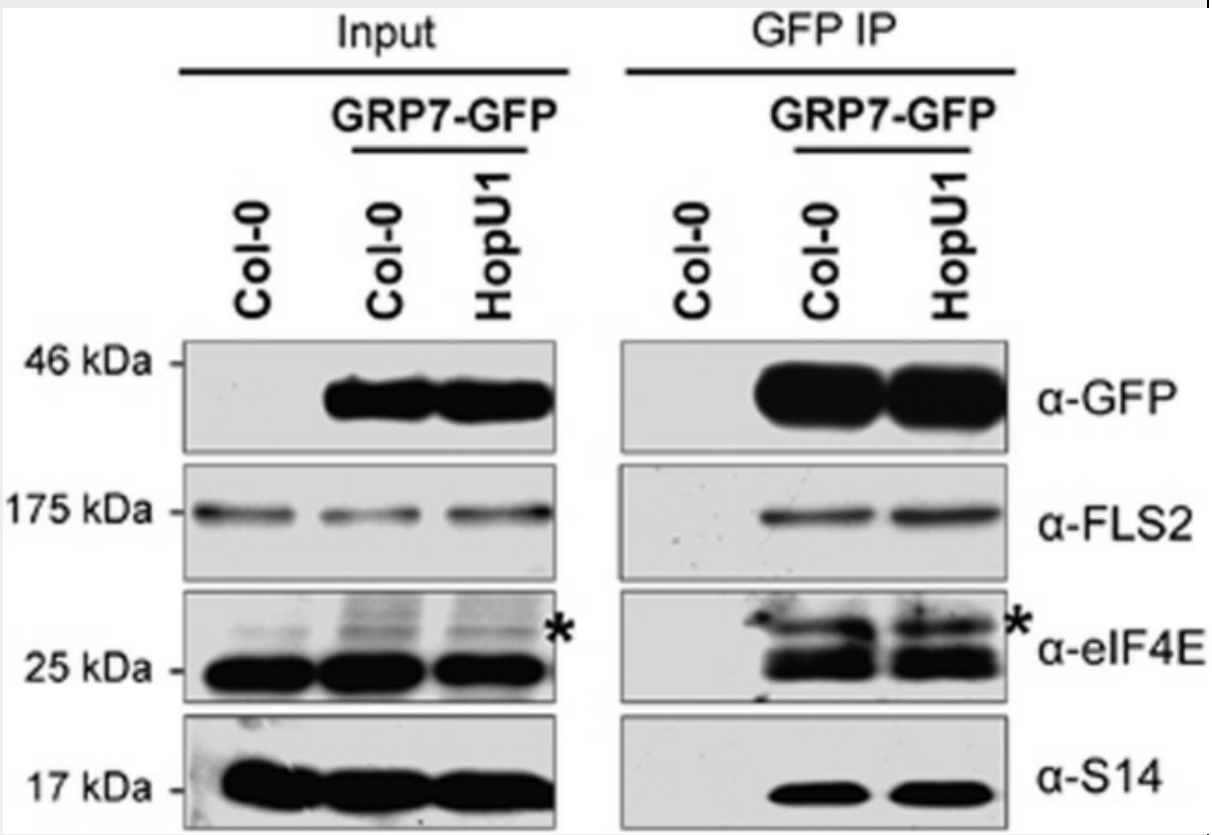

Figure 4.

HopU1 does not affect the protein–protein interactions between GRP7, FLS2 and translational components. Co-immunoprecipitation of GRP7-associated proteins in the presence of HopU1 in *A. thaliana*. Co-immunoprecipitation assay performed on Col-0 and HopU1 plants expressing or not GRP7-GFP. Total proteins (input) were subjected to immunoprecipitation with GFP Trap beads followed by immunoblot analysis with anti-GFP antibodies to detect GRP7 or specific antibodies recognizing FLS2, the translation initiation factor eIF4E, or the ribosomal protein S14. Asterisks mark slower migrating band forms. The results shown are representative of three independent experiments.

[Back]

[Back]

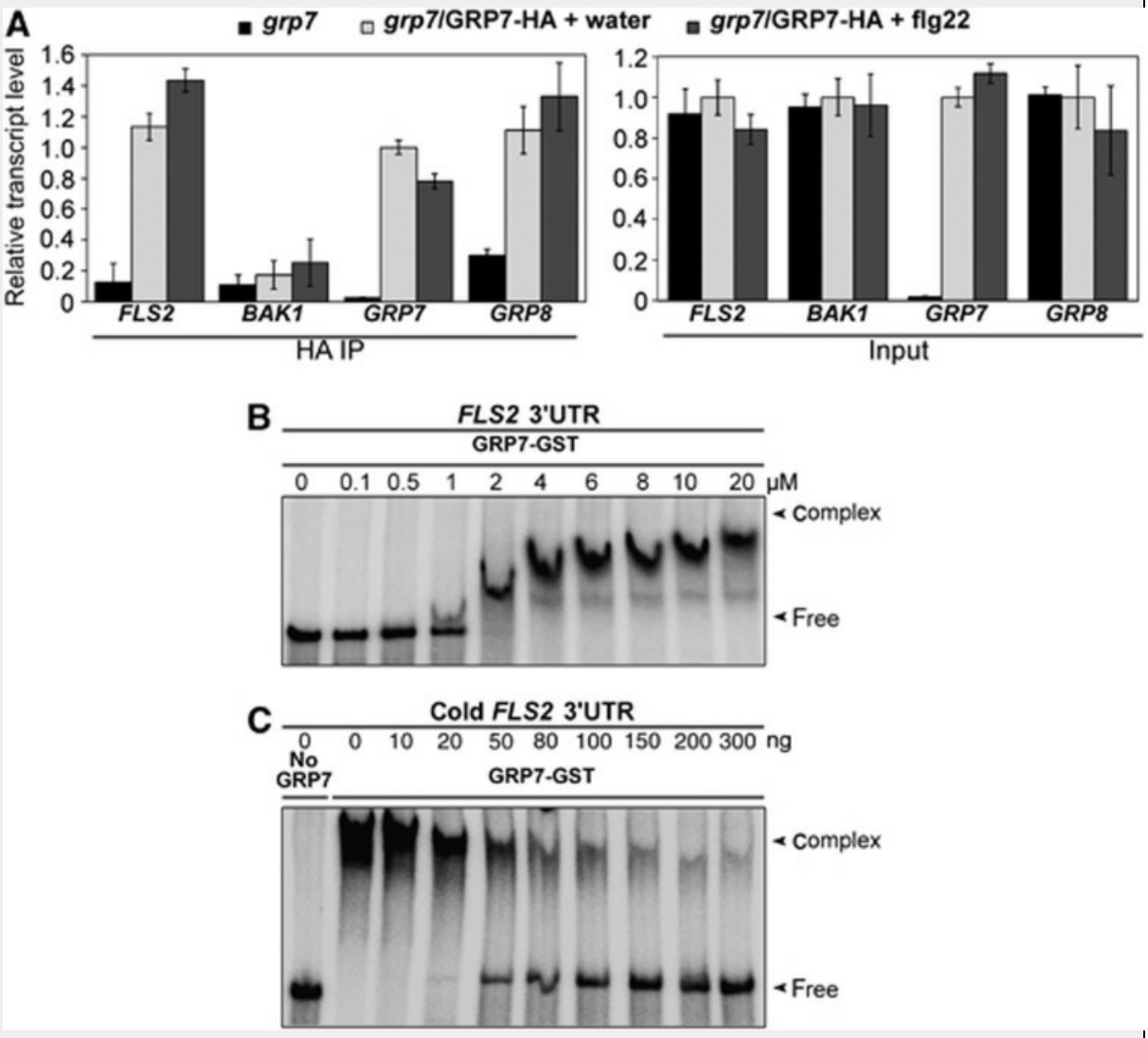

Figure 5.

GRP7 binds *FLS2* transcript. (**A**) RNA immunoprecipitation in *grp7-1* and *grp7-1*/GRP7-HA *A. thaliana* lines treated for 30 min with water or 1 µM flg22. Total proteins were subjected to immunoprecipitation with anti-HA antibodies followed by quantitative RT–PCR analysis of *FLS2*, *BAK1*, *GRP7* and *GRP8* transcripts with specific primers. Values are mean±s.e. (*n*=4). The results shown are representative of three independent experiments. (**B**, **C**) GRP7 binds the 3′UTR of *FLS2* transcripts *in vitro*. Electrophoretic shift assays performed on the 3′UTR of *FLS2* RNAs, in presence of increasing concentrations of GRP7-GST (**B**). Competition assay was performed with increasing quantity of unlabelled *FLS2* 3′UTR transcripts to GRP7-GST and ^{32}P-labelled *FLS2* 3'UTR transcripts (**C**). The results shown are representative of three independent experiments.

[Back]

[Back]

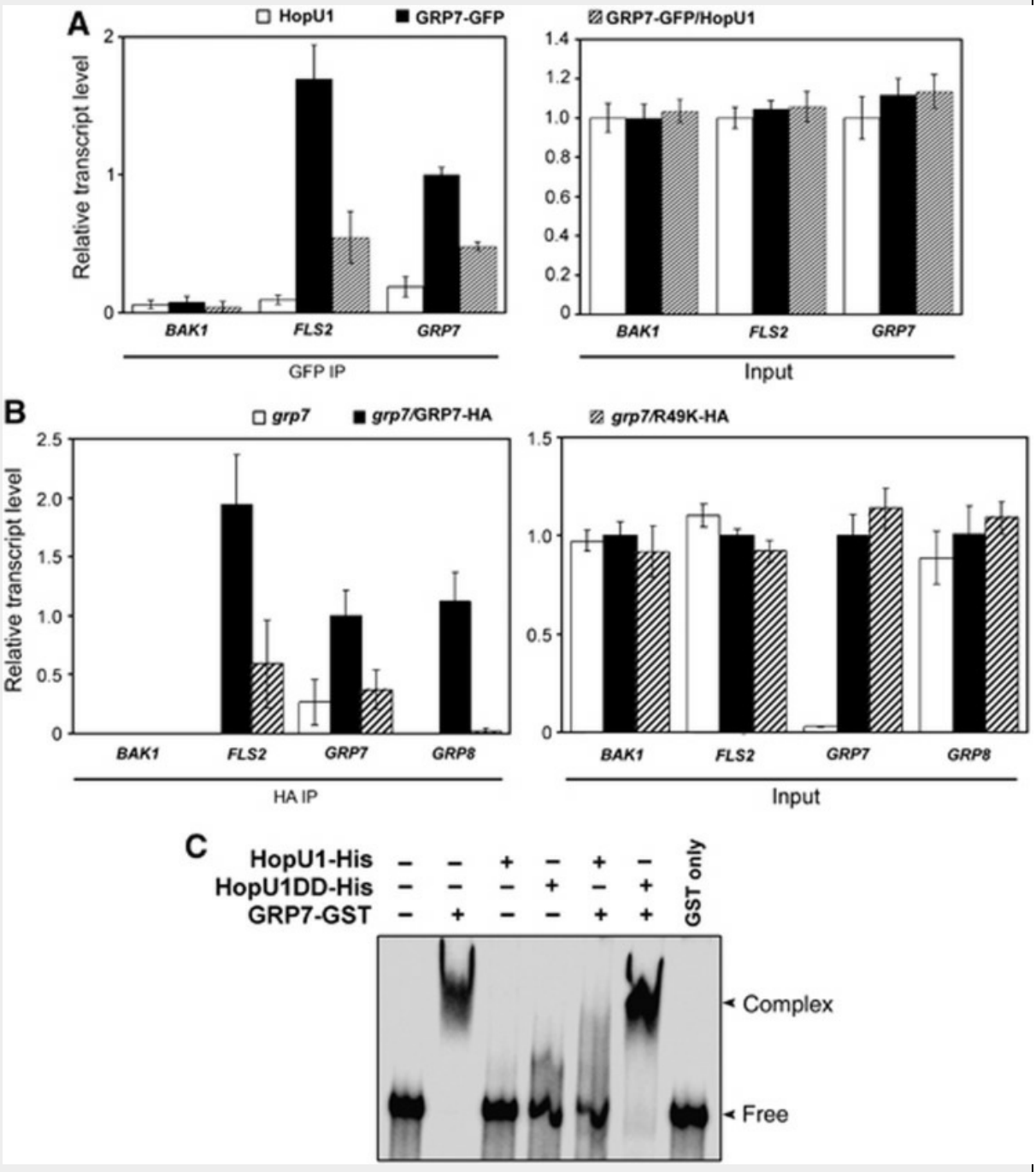

Figure 6.

HopU1 disrupts GRP7–*FLS2* transcripts interactions. (**A**) RNA immunoprecipitation in HopU1, GRP7-GFP and GRP7-GFP/HopU1 *A. thaliana* lines. Total proteins were subjected to immunoprecipitation with GFP Trap beads followed by quantitative RT–PCR analysis of *BAK1*, *FLS2* and *GRP7* transcripts with specific primers. Values

are mean±s.e. (*n*=4). (**B**) RNA immunoprecipitation in *grp7*, *grp7/*GRP7-HA and *grp7/*GRP7(R49K)-HA *A. thaliana* lines. Total proteins were subjected to immunoprecipitation with anti-HA matrix beads followed by quantitative RT–PCR analysis of *BAK1*, *FLS2*, *GRP7* and *GRP8* transcripts with specific primers. Values are mean±s.e. (*n*=4). (**C**) Electrophoretic shift assays in the presence of HopU1 and its inactive version HopU1DD. Standard ADP-ribosylation reaction was performed with 4 μM GRP7-GST in the presence of 1 μM HopU1 or HopU1DD. The corresponding GRP7-GST was then added to the 3′-UTR of *FLS2* transcript binding assay. The results shown are representative of three independent experiments.

[Back]

[Back]

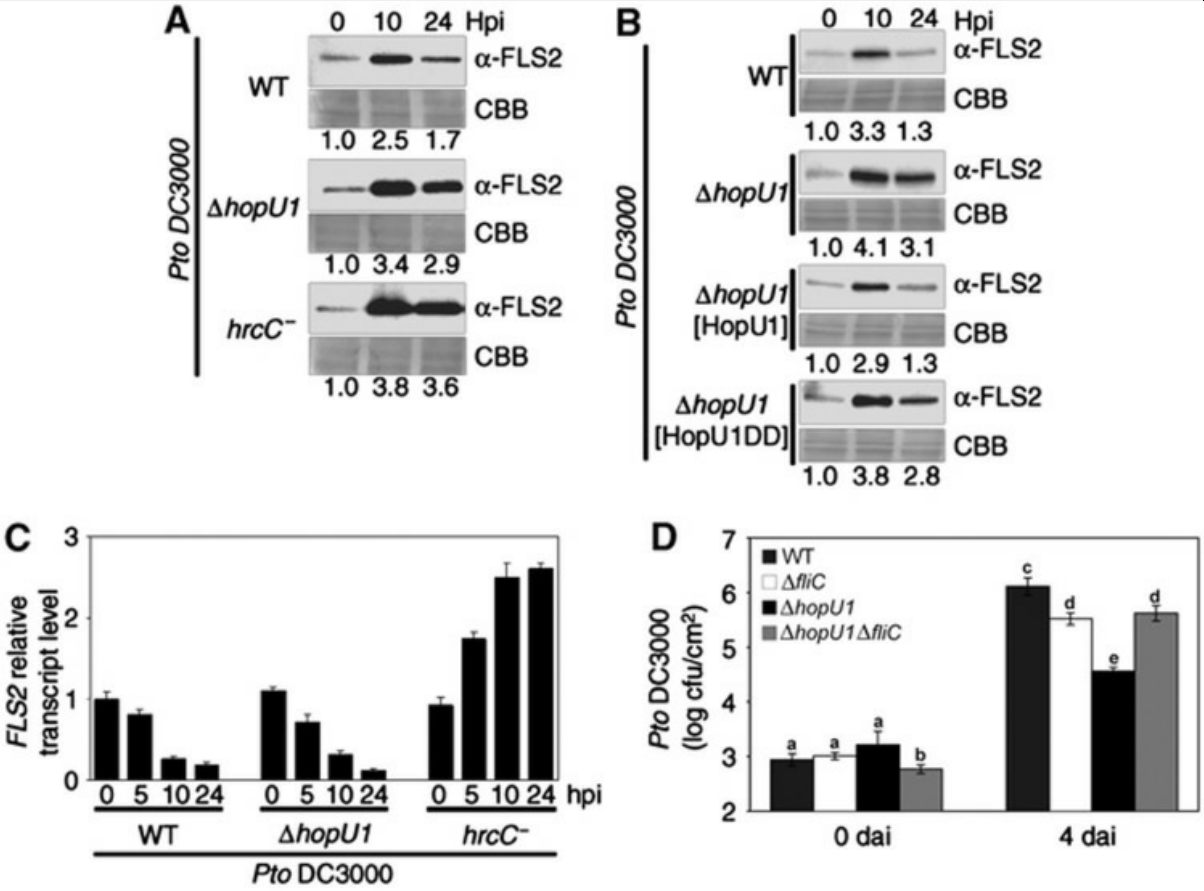

Figure 7.

HopU1 inhibits FLS2 protein accumulation during infection. (**A**) Immunoblots with specific antibodies detecting endogenous FLS2 in Col-0 during bacterial infection after syringe inoculation with *Pto* DC3000 (WT; inoculum: 5 × 10^7 cfu/ml), *Pto* DC3000 Δ*hopU1* (inoculum: 10^8 cfu/ml), *Pto* DC3000 *hrcC*⁻ (inoculum: 10^8 cfu/ml). hpi, hours post infection; CBB, Coomassie Brilliant Blue. Values correspond to signal intensity of the FLS2-specific band from the immunoblots relative to the zero time point. (**B**) Immunoblots with specific antibodies detecting endogenous FLS2 in Col-0 during bacterial infection after syringe inoculation with *Pto* DC3000 (WT; inoculum: 5 × 10^7 cfu/ml), *Pto* DC3000 Δ*hopU1* (inoculum: 10^8 cfu/ml), *Pto* DC3000 Δ*hopU1* [HopU1] (inoculum: 10^8 cfu/ml), *Pto* DC3000 Δ*hopU1* [HopU1DD] (inoculum: 10^8 cfu/ml). hpi, hours post infection; CBB, Coomassie Brilliant Blue. Values correspond to signal intensity of the FLS2-specific band from the immunoblots relative to the zero time point. (**C**) *FLS2* transcript level as measured by quantitative RT–PCR in Col-0 plants during bacterial infection after syringe inoculation with *Pto* DC3000 (WT; inoculum: 5 × 10^7 cfu/ml), *Pto* DC3000 Δ*hopU1*

(inoculum: 10^8 cfu/ml), *Pto* DC3000 *hrcC*$^-$ (inoculum: 10^8 cfu/ml). hpi, hours post infection. (**D**) Bacterial growth measured during *Pseudomonas* infection in Col-0 plants, after spray inoculation (inoculum: 2×10^8 cfu/ml) with *Pto* DC3000 wild-type (WT) or the derivated strains Δ*fliC*, Δ*hopU1* and Δ*hopU1*Δ*fliC*. Growth measured by colony forming units (cfu) 4 days after inoculation. Values are mean±s.e. (*n*=4). Statistical significance was assessed using the ANOVA test ($P<0.001$; letters indicate statistically significant differences). dai, days after inoculation. The results shown are representative of three independent experiments.

[Back]

Table of Contents

Supplementary Information Nicaise et al., 2012

Supplemental figures

Figure S1. GRP7 over-expression in the GRP7ox line.

Immunoblots with a specific antibody detecting GRP7 in Col-2 and the transgenic *Arabidopsis thaliana* line overexpressing GRP7 (GRP7ox). The blot obtained with the antibody anti-LHCP (Light Harvesting Chlorophyll a/b Protein) served as a loading control.

Figure S2. HopU1 suppresses early and late immune responses triggered by flg22 in Arabidopsis.

(A) Oxidative burst triggered by 50 nM flg22 or 50 nM elf18 in Col-0 and transgenic *Arabidopsis thaliana* plants expressing HopU1-HA under 35S promoter (HopU1). ROS production is presented as total photon count during 40 min of treatment and measured in relative light units (RLU). Values are mean ± SE (n=12). Statistical significance was assessed using the ANOVA test (P<0.001).

(B) Callose deposition induced by 1 µM flg22 infiltrated in Col-0 and transgenic *Arabidopsis thaliana* plants expressing HopU1-HA under 35S promoter (HopU1). Values are mean ± SE (n=10). Statistical significance was assessed using the ANOVA test (P<0.001).

(C) Semi-quantitative immunoblot analysis with specific antibodies detecting endogenous FLS2 in Col-0 and transgenic *Arabidopsis thaliana* plants expressing HopU1-HA under 35S promoter (HopU1). Values correspond to signal intensity of the bands from the immunoblots relative to the undiluted sample from Col-0. CBB, Coomassie Brillant Blue. The results shown are representative of three out of four independent experiments.

(D) Oxidative burst triggered by 50 nM flg22 in Col-0 and transgenic *Arabidopsis thaliana* plants expressing HopU1-HA under the control of an estradiol-inducible promoter (ind_HopU1), with or without a 15 µM β-estradiol pre-treatment. ROS production is presented as total photon count during 40 min of treatment and measured in relative light units (RLU). Values are mean ± SE (*n*=12). Statistical significance was assessed using the ANOVA test (*P*<0.001).

(E) Callose deposition induced by 1 µM flg22 infiltrated in Col-0 and transgenic *Arabidopsis thaliana* plants expressing HopU1-HA under the control of an estradiol-inducible promoter (ind_HopU1), with or without a 15 µM β-estradiol pre-treatment. Values are mean ± SE (*n*=10). Statistical significance was assessed using the ANOVA test (*P*<0.001).

(F) Growth of *Pseudomonas syringae* pv. *tomato* (*Pto*) DC3000 on Col-0, HopU1 (35S::HopU1-HA) and *fls2* plants as measured by colony forming units (cfu). Bacterial growth was measured three days after spray-inoculation with wild-type *Pto* DC3000 (WT; inoculum: 10^6 cfu/mL), *Pto* DC3000 *ΔhopU1* (inoculum: 10^8 cfu/mL) and *Pto DC3000 hrcC*$^-$ (inoculum: 10^8 cfu/mL). Values are mean ± SE (*n*=4). Statistical significance was assessed using the ANOVA test (*P*<0.05).

(G) Growth of *Pseudomonas syringae* pv. *tomato* (*Pto*) DC3000 wild-type and the strain *ΔhopU1* on Col-2 and the transgenic plants overexpressing GRP7 (GRP7ox), as measured by colony forming units (cfu). Bacterial growth was measured four days after spray-inoculation with wild-type DC3000 (WT; inoculum: 10^8 cfu/mL) and DC3000 *ΔhopU1* (inoculum: 10^8 cfu/mL). Values are mean ± SE (*n*=4). Statistical significance was assessed using the ANOVA test (*P*<0.05).

All results shown are representative of at least three independent experiments.

Figure S3. GRP7 interacts with EFR at the plasma membrane.

(A) EFR and GRP7 interact in yeast two-hybrid assays. The cytoplasmic part of *EFR* (EFRcyt) has been found to interact with GRP7 during a yeast two-hybrid screen and

confirmed upon expression of pLexA-EFRcyt and pB42AD-GRP7. Interaction assays were performed in presence or absence of the auxotrophic amino acid leucine (Leu).

(B) Bimolecular fluorescence complementation assays between GRP7 and EFR. YFPn, GRP7-YFPn, YFPc and EFR-YFPc, as well as the reverse combinations YFPc, GRP7-YFPc, YFPn and EFR-YFPn, were transiently co-expressed in *N. benthamiana* leaves. The chlorophyll autofluorescence appears in red. Scale bar corresponds to 20 µm. Photographs were taken 2 days after infiltration and are representative of the total observations (*n*=60).

All results shown are representative of three independent experiments.

Figure S4. GRP7 sub-cellular localisation.

(A) GRP7 sub-cellular localisation in the stable transgenic on *Arabidopsis thaliana* plants *35S::GRP7-GFP* line as observed by confocal microscopy. The chlorophyll autofluorescence appears in red.

(B) Localisation of GRP7-eGFP transiently expressed in *N. benthamiana* and *N. tabacum* as observed by confocal microscopy. The chlorophyll autofluorescence appears in red.

All results shown are representative of three independent experiments.

Figure S5. HopU1 does not interact with, nor ADP-ribosylates FLS2 protein.

(A) Co-immunoprecipitation assay performed after transient co-expression of HopU1-HA and FLS2-GFP-His on *N. benthamiana* plants, with (+) or without (-) treatment of the samples with 1 µM flg22 during 15 min. Total proteins (input) were subjected to immunoprecipitation with anti-HA beads followed by immunoblot analysis.

(B) Bimolecular fluorescence complementation assays between HopU1 and FLS2. HopU1-YFPn and FLS2-YFPc, as well as the opposite combination HopU1-YFPc and FLS2-YFPn, were transiently co-expressed *N. benthamiana* leaves. The chlorophyll autofluorescence appears in red. Scale bar corresponds to 20 µm.

Photographs were taken 2 days after infiltration and are representative of the total observations (*n*=60).

(C) *In vitro* ADP-ribosylation assay performed with recombinant FLS2-GST and HopU1-His on supernatant (sup.) and pellet (pell.) fractions. The reaction between GRP7-GST and HopU1-His has been included as a positive control.

All results shown are representative of three independent experiments.

Figure S6. GRP7 interacts with HopU1 in the cytoplasm and in the nucleus.

(A) Co-immunoprecipitation of GRP7 and HopU1. GRP7-eGFP and HopU1-HA were transiently co-expressed in *N. benthamiana* leaves. Total proteins (input) were subjected to immunoprecipitation with anti-HA beads followed by immunoblot analysis with anti-GFP antibodies to detect GRP7-eGFP.

(B) Bimolecular fluorescence complementation assays between GRP7 and HopU1. GRP7-YFPn and HopU1-YFPc, as well as the opposite combination GRP7-YFPc and HopU1-YFPn, were transiently co-expressed *N. benthamiana* leaves. The chlorophyll autofluorescence appears in red. Scale bar corresponds to 20 µm. Photographs were taken 2 days after infiltration and are representative of the total observations (n=60).

All results shown are representative of three independent experiments.

Figure S7. HopU1 does not affect the elicitation-dependent dissociation of eIF4E or S14 translational components from the GRP7 immunoprecipitates.

Co-immunoprecipitation assay performed on Col-0/GRP7-GFP plants expressing the effector HopU1, untreated (-) or treated (+) with 1µM flg22 for 15 min. Total proteins (input) were subjected to immunoprecipitation with GFP Trap beads followed by immunoblot analysis with anti-GFP antibodies to detect GRP7-GFP or specific antibodies recognizing the translation initiation factor eIF4E or the ribosomal protein

S14. Asterisks mark slower-migrating bands forms. The results shown are representative of three independent experiments.

Figure S8. HopU1 disrupts GRP7-*EFR* transcripts interactions.

(A) RNA immunoprecipitation in HopU1-HA, GRP7-GFP and GRP7-GFP/HopU1-HA *Arabidopsis thaliana* lines. Total proteins were subjected to immunoprecipitation with GFP Trap beads followed by quantitative RT-PCR analysis of *BAK1*, *EFR*, and *GRP7* transcripts with specific primers. Values are mean ± SE (*n*=4).

(B) RNA immunoprecipitation in *grp7*, *grp7/*GRP7-HA and *grp7/*GRP7(R49K)-HA *Arabidopsis thaliana* lines. Total proteins were subjected to immunoprecipitation with anti-HA matrix beads followed by quantitative RT-PCR analysis of *BAK1*, *EFR*, *GRP7* and *GRP8* transcripts with specific primers. Values are mean ± SE (*n*=4).

Figure S9. GRP8 also binds *FLS2* and *EFR* transcripts.

RNA immunoprecipitation in Col-0 and GRP8-HA *Arabidopsis thaliana* lines. Total proteins were subjected to immunoprecipitation with anti-HA beads followed by quantitative RT-PCR analysis of *BAK1*, *EFR*, *FLS2*, *GRP7* and *GRP8* transcripts with specific primers. Values are mean ± SE (*n*=4).

Figure S10. HopU1 does not affect BAK1 protein accumulation during infection.

Immunoblots with specific antibodies detecting endogenous BAK1 or FLS2 in Col-0 during bacterial infection after syringe-inoculation with *Pto* DC3000 (WT; inoculum: $5x10^7$ cfu/mL), *Pto* DC3000 *ΔhopU1* (inoculum: 10^8 cfu/mL), *Pto* DC3000 *hrcC*$^-$ (inoculum: 10^8 cfu/mL). hpi, hours post-infection; CBB, Coomassie Brillant Blue. Values correspond to signal intensity of the FLS2-specific band from the immunoblots relative to the zero time-point.

Figure S11. GRP7 over-expression leads to increased FLS2 accumulation upon flg22 treatment.

(A) Immunoblots with specific antibodies detecting endogenous FLS2 protein in Col-2 and the transgenic plants overexpressing GRP7 (GRP7ox), untreated (-) or treated (+) with 1µM flg22 for 4 hours. CBB, Coomassie Brillant Blue.

(B) Quantification of FLS2 protein level in Col-2 and the transgenic plants overexpressing GRP7 (GRP7ox), untreated (-) or treated (+) with 1 µM flg22 for 4 hours. The histogram represents the average of the FLS2 relative band intensity compared to Col-0 (-) measured in three independent experiments. Values are mean ± SE (n=3). Statistical significance was assessed using the ANOVA test (P<0.05).

Supplementary Table S1

Table S1. GRP7 interacting proteins identified by GRP7-HA co-immunoprecipitation.

Protein	Accession number	GRP7:HA Co-IP #1	GRP7:HA Co-IP #2	GRP7:HA Co-IP #3	Col-0 Co-IP #1	Col-0 Co-IP #2	Col-0 Co-IP #3
GRP7	gi|15226605	68 (4030)	28 (1937)	84 (5247)			2 (127)
GRP8	gi|30692258	5 (140)	5 (119)	13 (162)			
eEF1A	gi|295789	3 (85)	6 (128)	5 (121)			1 (49)
eIF4A1 or eIF4A2	gi|79313227 or gi|15221761	4 (85)	2 (48)	2 (78)			
chloroplast EF-Tu precursor	gi|23397095	8 (570)	11 (686)	12 (811)	2 (168)	1 (100)	2 (165)
ATMS1 (methionine synthase 1)	gi|15238686	21 (749)	16 (465)	18 (801)	3 (57)		3 (48)
ATMS2 (methionine synthase 2)	gi|15228634	13 (560)	8 (247)	15 (651)			
ATMS3 (methionine synthase 3)	gi|30688090 or gi|55670112	3 (614)	15 (443)	8 (407)			2 (39)
ATP synthase CF1 beta subunit (ATPB)	gi|7525040	15 (614)	14 (663)	15 (727)			5 (264)
ATP synthase CF1 alpha subunit (ATPA)	gi|7525018	10 (494)	6 (163)	6 (253)	1 (65)		2 (58)
peroxisomal glycolate oxidase	gi|15231850	12 (470)	8 (399)	15 (710)			1 (45)
phosphoglycerate kinase	gi|1022805	9 (398)	4 (154)	10 (524)	3 (128)		2 (81)
Rubisco large subunit	gi|7525041	25 (849)	12 (408)	17 (519)	13 (451)		7 (226)
RCA (RUBISCO ACTIVASE)	gi|18405145	16 (534)	21 (717)	30 (1448)	3 (141)	4 (171)	16 (630)
GAPA (glyceraldehyde 3-phosphate dehydrogenase A subunit)	gi|166702	13 (559)	12 (600)	15 (653)	5 (190)	3 (81)	3 (104)
GAPA-2	gi|15222111	10 (532)	11 (587)	15 (719)		3 (72)	4 (138)
GAPB	gi|336390	12 (439)	15 (715)	20 (766)	7 (278)	2 (45)	6 (270)
GAPC1 or GAPC2	gi|15229231 or gi|15222848	9 (310)	10 (302)	10 (361)	2 (92)	2 (111)	2 (97)
HSP93-III	gi|186510816		10 (287)	6 (221)			
60 kDa Chaperonin or CPN60B	gi|15222729 or gi|15231255	1 (62)	1 (60)	4 (74)			
PATL1 (PATELLIN 1); transporter	gi|15218382	2 (57)	1 (34)	1 (43)			
MTO3 (methionine over-accumulator 3)	gi|15229033		1 (67)	1 (66)			
transketolase-like protein	gi|7329685	14 (557)	1 (96)	4 (110)			
ACTIN 1*	gi|166582	2 (114)		5 (113)			1 (67)
ACTIN 7*	gi|15242516	2 (60)		7 (243)			
ACTIN 8*	gi|1669389	2 (60)	2 (82)	5 (178)			
myosin heavy chain-related	gi|15238179		1 (35)	1 (36)			
putative alanine aminotransferase	gi|13430566		2 (41)	2 (92)			
GS2 (GLUTAMINE SYNTHETASE 2)	gi|15238559		2 (66)	4 (147)			
AGT (ALANINE:GLYOXYLATE AMINOTRANSFERASE)	gi|15225026		1 (82)	1 (39)			

GRP7 interacting proteins were isolated from transgenic GRP7-HA plants using anti-HA beads, and identified with tandem mass spectrometry. Listed are all peptides present specifically in the GRP7-HA plants compared to the Col-0 control plants, identified at least twice in three independent experiments (probability of 95% or higher, equivalent to ion score of 32 or higher based on Mascot program). For each identified protein, the number of peptides is listed. The ion scores are listed in the parenthesis.
*The actin sequences can be shared with other actin isoforms with equal or less probability.

Figure S1

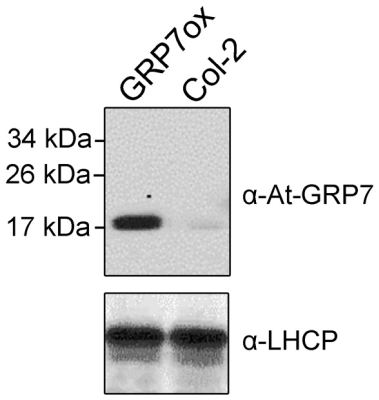

Figure S2

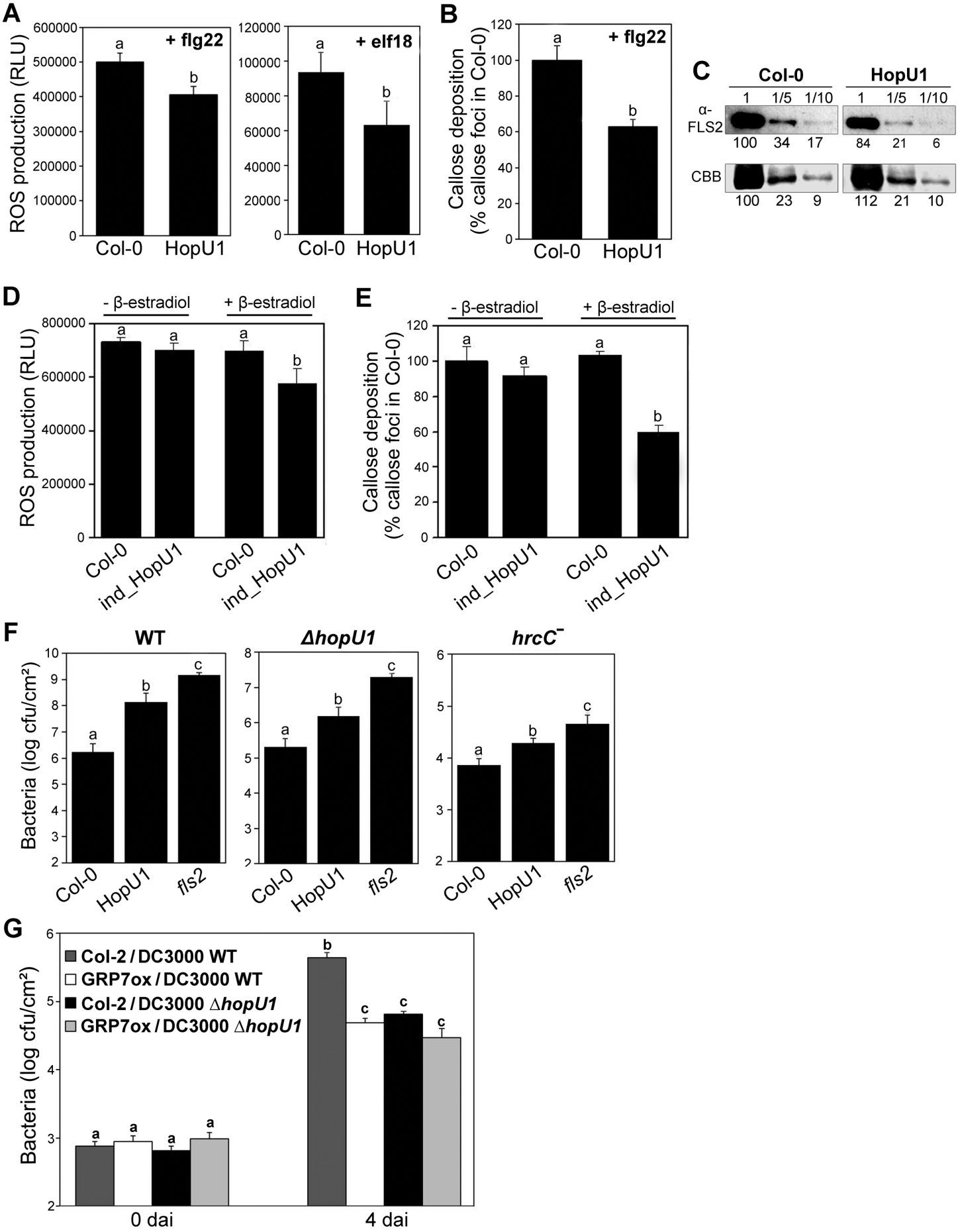
A
ROS production (RLU)
+ flg22
+ elf18
Col-0
HopU1
B
Callose deposition (% callose foci in Col-0)
+ flg22
C
Col-0
HopU1
1
1/5
1/10
α-FLS2
100 34 17
84 21 6
CBB
100 23 9
112 21 10
D
- β-estradiol
+ β-estradiol
ROS production (RLU)
Col-0
ind_HopU1
E
Callose deposition (% callose foci in Col-0)
F
WT
ΔhopU1
hrcC⁻
Bacteria (log cfu/cm²)
Col-0
HopU1
fls2
G
Col-2 / DC3000 WT
GRP7ox / DC3000 WT
Col-2 / DC3000 ΔhopU1
GRP7ox / DC3000 ΔhopU1
Bacteria (log cfu/cm²)
0 dai
4 dai

Figure S3

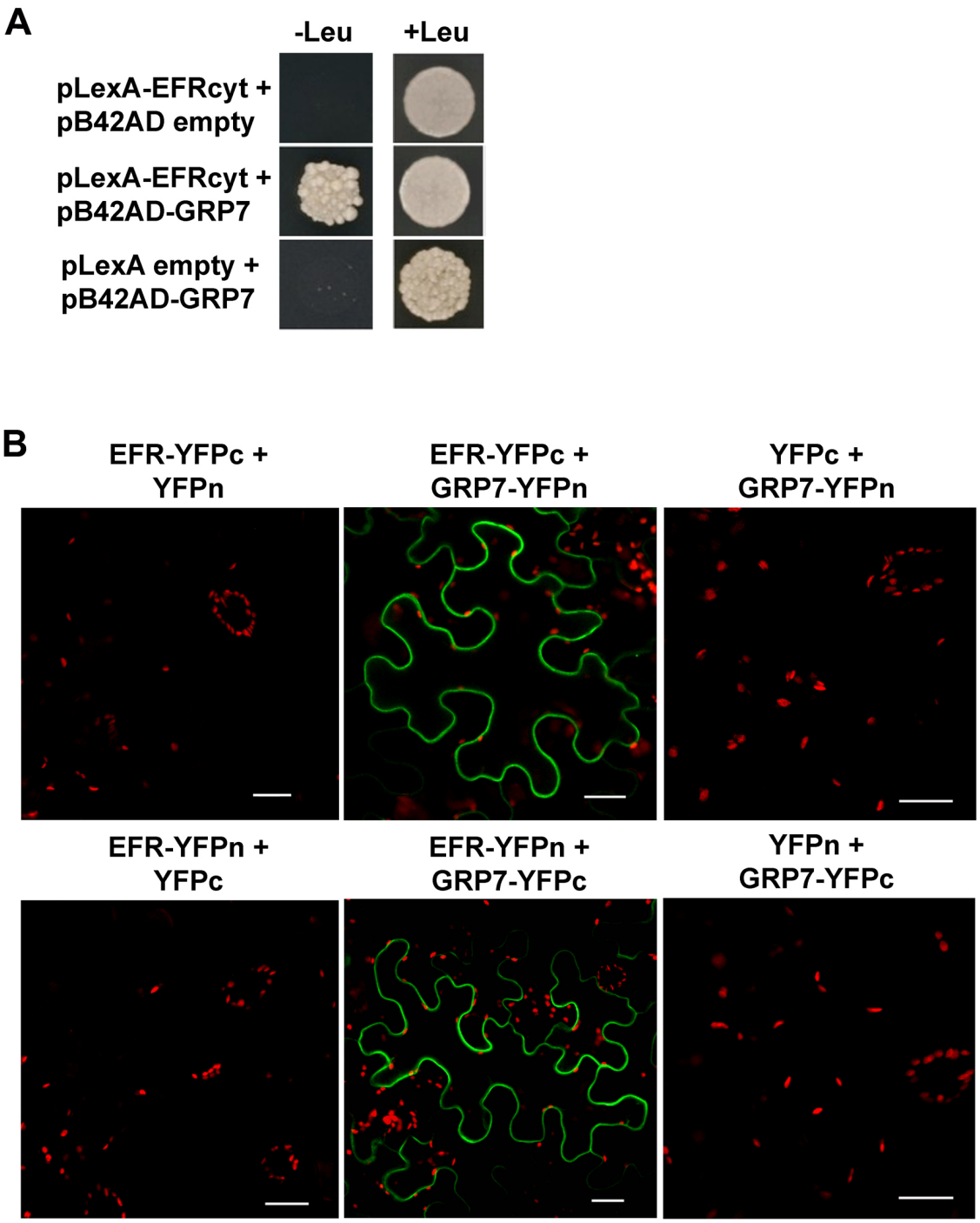
A
-Leu
+Leu
pLexA-EFRcyt + pB42AD empty
pLexA-EFRcyt + pB42AD-GRP7
pLexA empty + pB42AD-GRP7
B
EFR-YFPc + YFPn
EFR-YFPc + GRP7-YFPn
YFPc + GRP7-YFPn
EFR-YFPn + YFPc
EFR-YFPn + GRP7-YFPc
YFPn + GRP7-YFPc

Figure S4

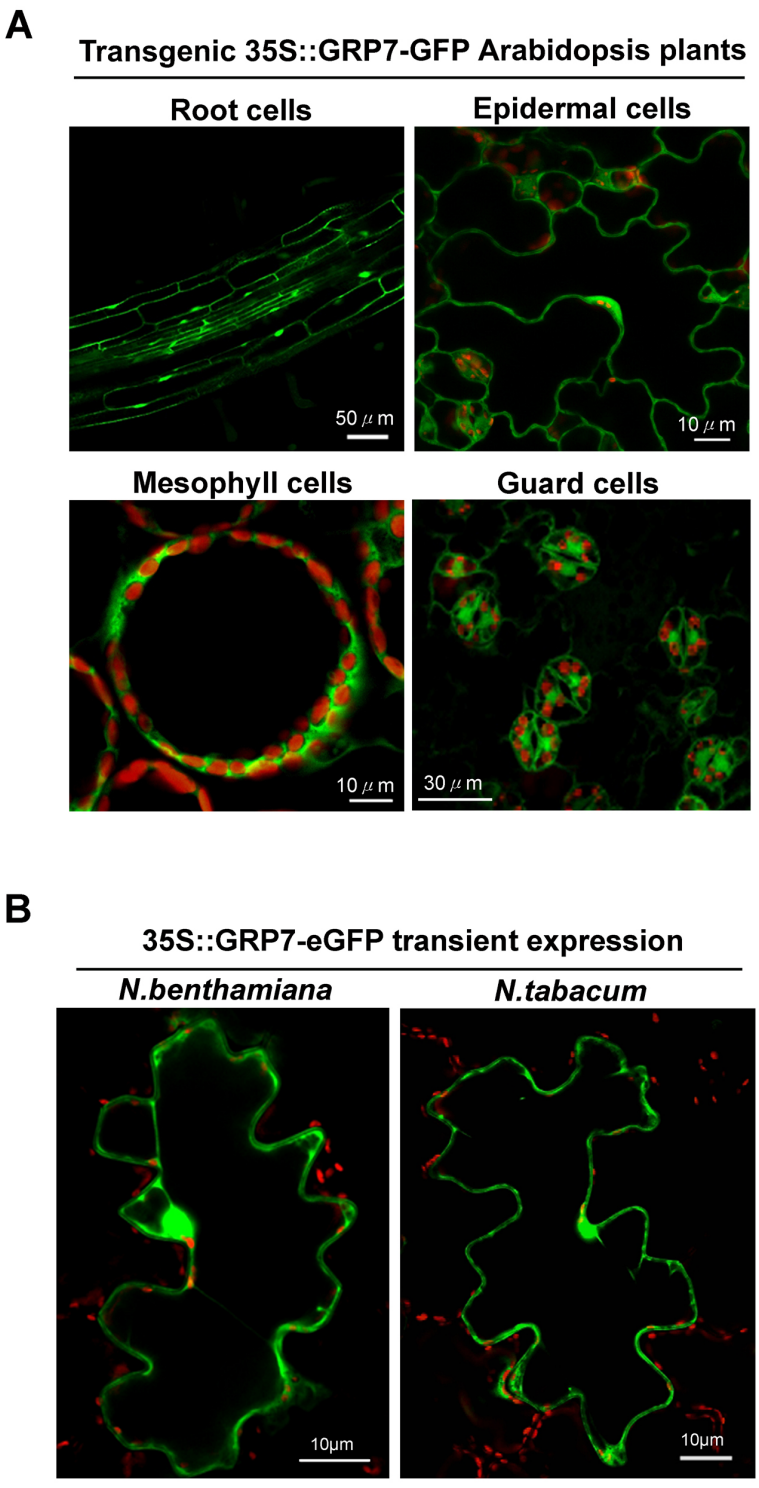
A
Transgenic 35S::GRP7-GFP Arabidopsis plants
Root cells
Epidermal cells
50 μm
10 μm
Mesophyll cells
Guard cells
10 μm
30 μm
B
35S::GRP7-eGFP transient expression
N.benthamiana
N.tabacum
10μm
10μm

Figure S5

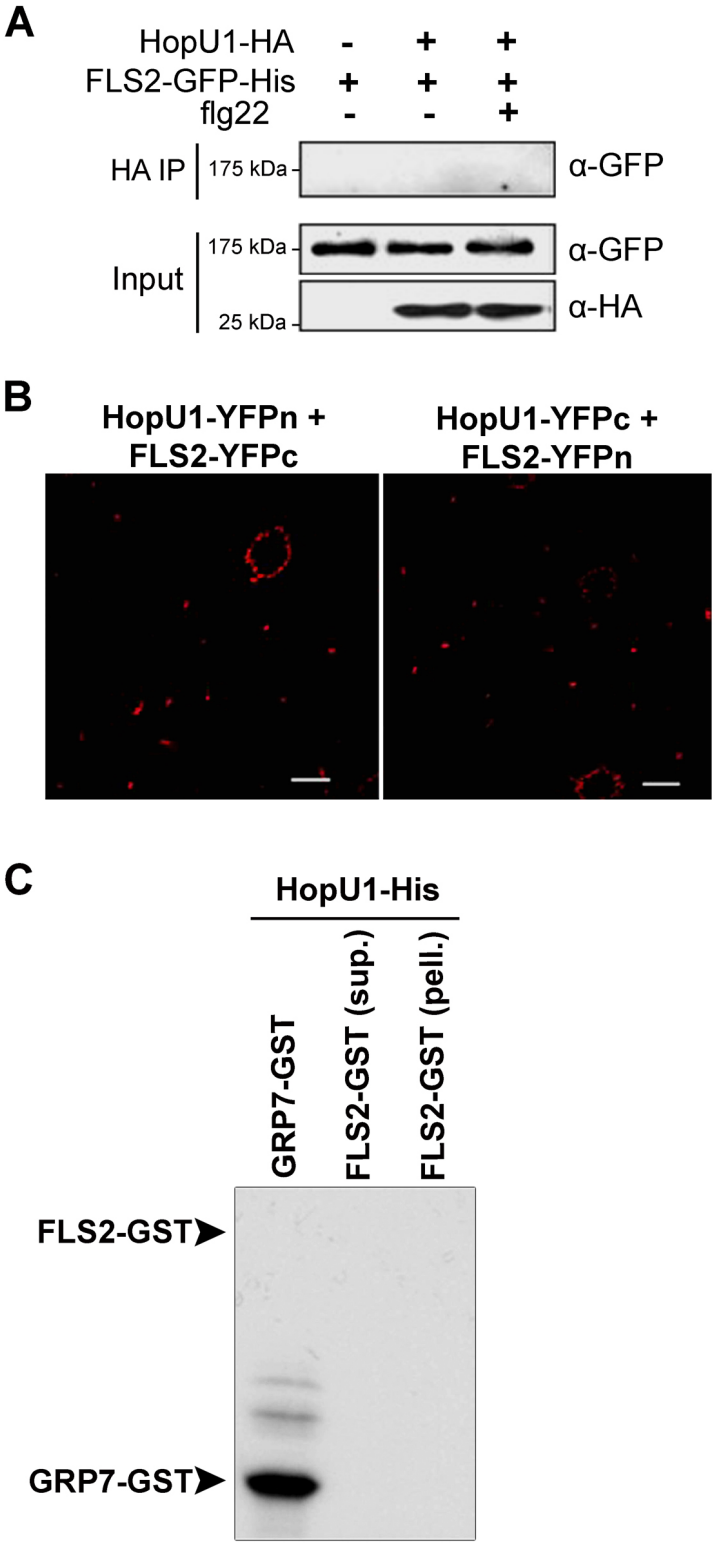
A
HopU1-HA - + +
FLS2-GFP-His + + +
flg22 - - +
HA IP
175 kDa
α-GFP
Input
175 kDa
α-GFP
25 kDa
α-HA
B
HopU1-YFPn + FLS2-YFPc
HopU1-YFPc + FLS2-YFPn
C
HopU1-His
GRP7-GST
FLS2-GST (sup.)
FLS2-GST (pell.)
FLS2-GST
GRP7-GST

Figure S6

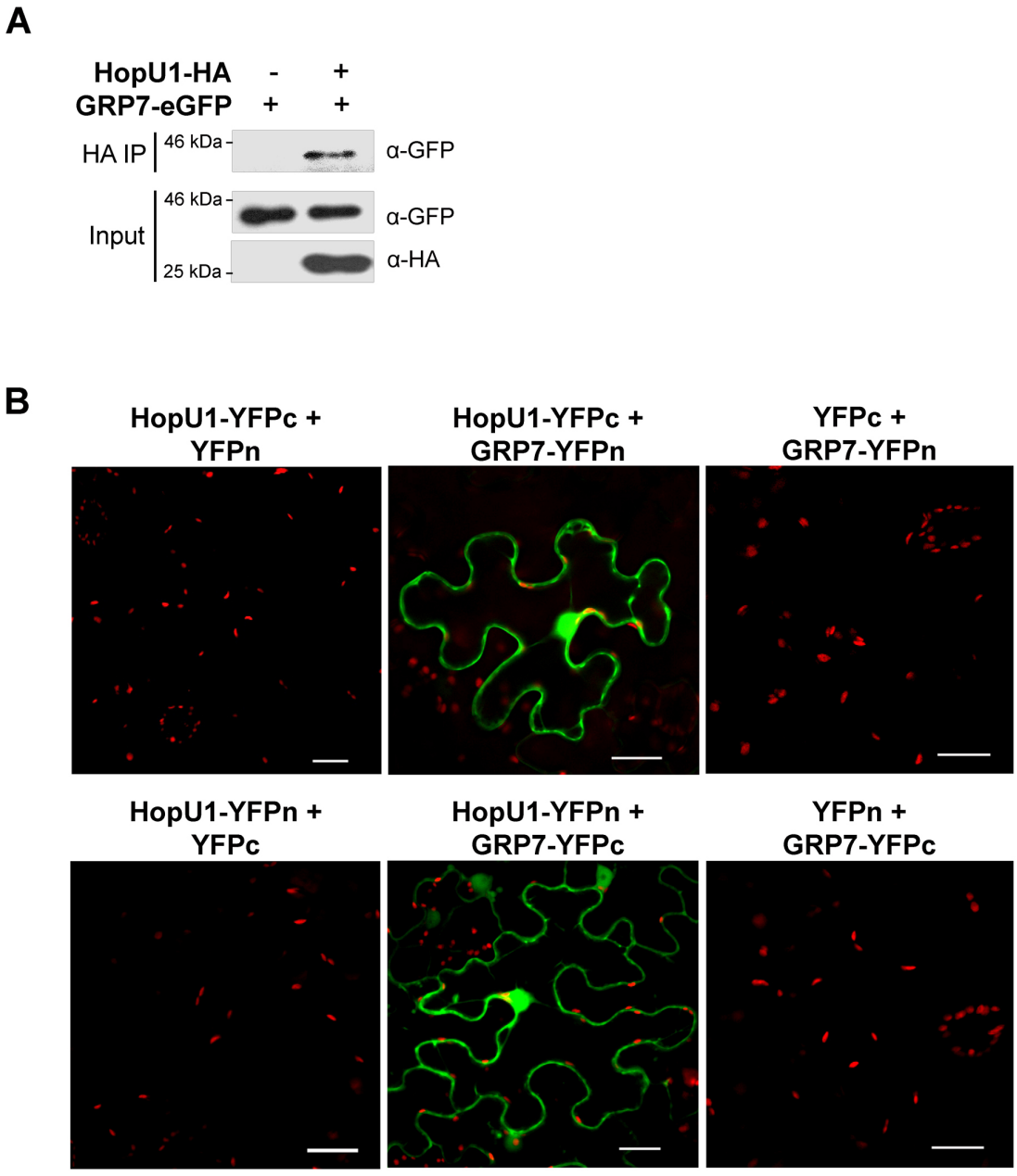
A
HopU1-HA - +
GRP7-eGFP + +
HA IP
46 kDa
α-GFP
Input
46 kDa
α-GFP
25 kDa
α-HA
B
HopU1-YFPc + YFPn
HopU1-YFPc + GRP7-YFPn
YFPc + GRP7-YFPn
HopU1-YFPn + YFPc
HopU1-YFPn + GRP7-YFPc
YFPn + GRP7-YFPc

Figure S7

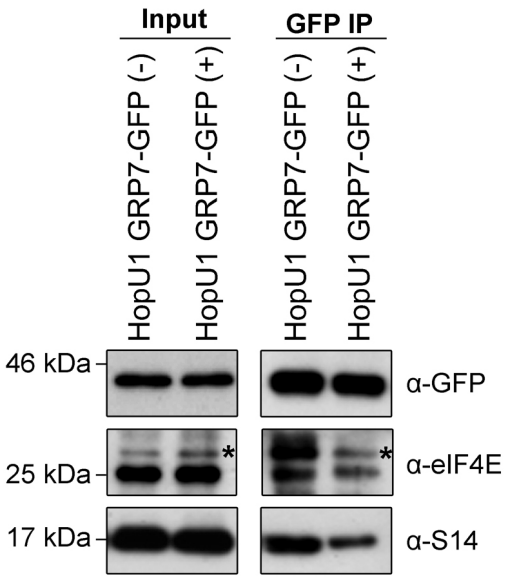
Input
GFP IP
HopU1 GRP7-GFP (-)
HopU1 GRP7-GFP (+)
HopU1 GRP7-GFP (-)
HopU1 GRP7-GFP (+)
46 kDa
25 kDa
17 kDa
α-GFP
α-eIF4E
α-S14
*
*

Figure S8

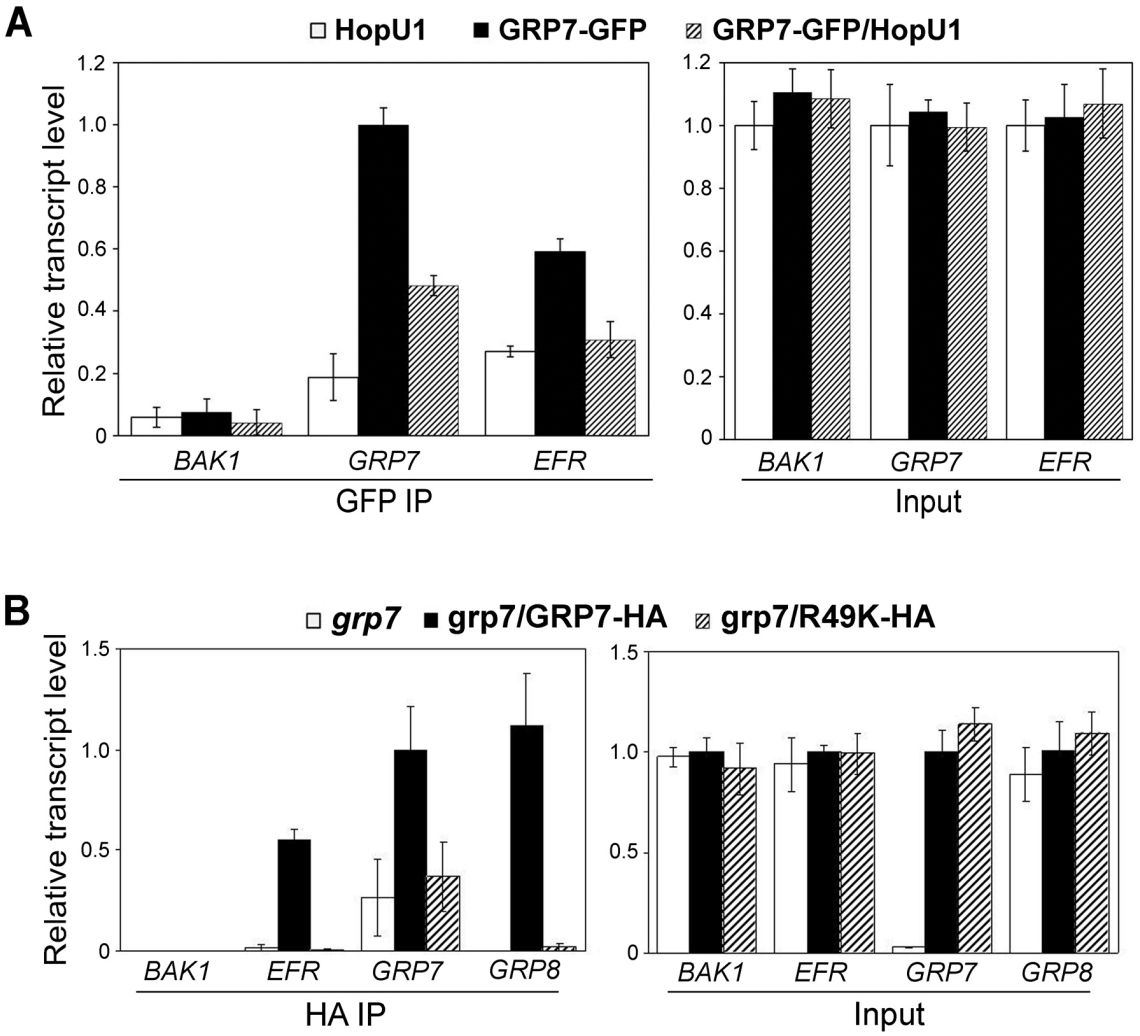
A
HopU1
GRP7-GFP
GRP7-GFP/HopU1
Relative transcript level
1.2
1.0
0.8
0.6
0.4
0.2
0
BAK1
GRP7
EFR
GFP IP
Input
B
grp7
grp7/GRP7-HA
grp7/R49K-HA
1.5
0.5
GRP8
HA IP

Figure S9

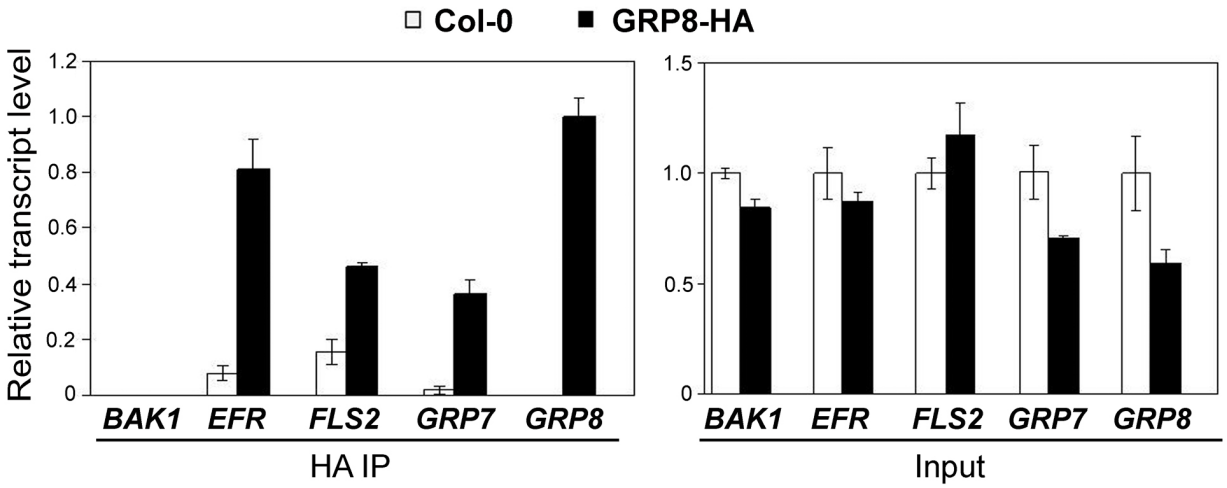
Col-0
GRP8-HA
Relative transcript level
1.2
1.0
0.8
0.6
0.4
0.2
0
BAK1
EFR
FLS2
GRP7
GRP8
HA IP
1.5
1.0
0.5
0
BAK1
EFR
FLS2
GRP7
GRP8
Input

Figure S10

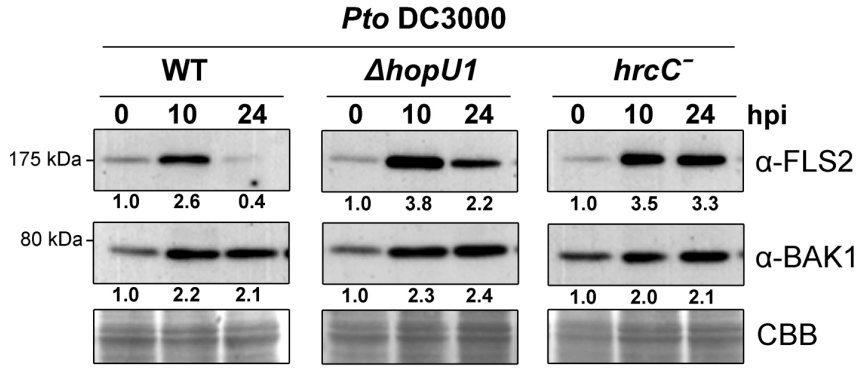
Pto DC3000
WT
ΔhopU1
hrcC⁻
0 10 24 0 10 24 0 10 24 hpi
175 kDa
1.0 2.6 0.4
1.0 3.8 2.2
1.0 3.5 3.3
α-FLS2
80 kDa
1.0 2.2 2.1
1.0 2.3 2.4
1.0 2.0 2.1
α-BAK1
CBB

Figure S11

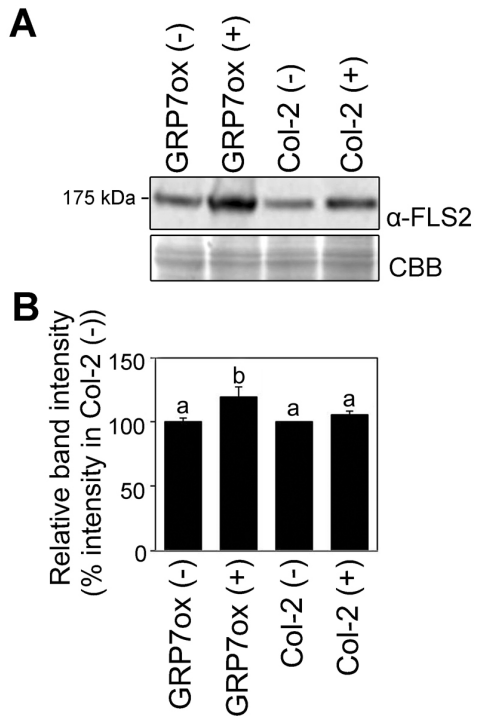
A
GRP7ox (-)
GRP7ox (+)
Col-2 (-)
Col-2 (+)
175 kDa
α-FLS2
CBB
B
Relative band intensity
(% intensity in Col-2 (-))
150
100
50
0
a
b
a
a
GRP7ox (-)
GRP7ox (+)
Col-2 (-)
Col-2 (+)